Visible and near-infrared multispectral analysis of geochemically measured rock fragments at the Opportunity landing site in Meridiani Planum

Catherine M. Weitz,[1] William H. Farrand,[2] Jeffrey R. Johnson,[3] Iris Fleischer,[4] Christian Schröder,[5,6] Aileen Yingst,[1] Brad Jolliff,[7] Ralf Gellert,[8] Jim Bell,[9] Kenneth E. Herkenhoff,[3] Göstar Klingelhöfer,[4] Barbara Cohen,[10] Wendy Calvin,[11] Malcolm Rutherford,[12] and James Ashley[13]

Received 25 May 2010; revised 28 July 2010; accepted 12 August 2010; published 20 November 2010.

[1] We have used visible and near-infrared Panoramic Camera (Pancam) spectral data acquired by the Opportunity rover to analyze 15 rock fragments at the Meridiani Planum landing site. These spectral results were then compared to geochemistry measurements made by the in situ instruments Mössbauer (MB) and Alpha Particle X-ray Spectrometer (APXS) to determine the feasibility of mineralogic characterization from Pancam data. Our results suggest that dust and alteration rinds coat many rock fragments, which limits our ability to adequately measure the mineralogy of some rocks from Pancam spectra relative to the different field of view and penetration depths of MB and APXS. Viewing and lighting geometry, along with sampling size, also complicate the spectral characterization of the rocks. Rock fragments with the same geochemistry of sulfate-rich outcrops have similar spectra, although the sulfate-rich composition cannot be ascertained based upon Pancam spectra alone. FeNi meteorites have spectral characteristics, particularly ferric oxide coatings, that generally differentiate them from other rocks at the landing site. Stony meteorites and impact fragments with unknown compositions have a diverse range of spectral properties and are not well constrained nor diagnostic in Pancam data. Bounce Rock, with its unique basalt composition, is easily differentiated in the Pancam data from all other rock types at Meridiani Planum. Our Pancam analyses of small pebbles adjacent to these 15 rock fragments suggests that other rock types may exist at the landing site but have not yet been geochemically measured.

Citation: Weitz, C. M., et al. (2010), Visible and near-infrared multispectral analysis of geochemically measured rock fragments at the Opportunity landing site in Meridiani Planum, *J. Geophys. Res.*, *115*, E00F10, doi:10.1029/2010JE003660.

1. Introduction

[2] Fifteen rock fragments at the Opportunity landing site have been analyzed as of sol 2004 by both the rover visible and near-infrared Panoramic Camera (Pancam), and the in situ instruments, Mössbauer (MB) and Alpha Particle X-ray Spectrometer (APXS). Several of the rocks were large enough for the Rock Abrasion Tool (RAT) to either brush or grind, thereby exposing a fresher, cleaner surface. The rocks analyzed in this study include Bounce Rock, Lion Stone, Barberton, Heat Shield Rock, Russet, Arkansas, Perseverance, Antistasi, Santa Catarina, Santorini, Kos, Tilos, Rhodes, Kasos, and Block Island. Note that these names are informal and not approved by the International Astronomical Union. The rock fragments vary in size from pebbles (4–64 mm) and cobbles (64–256 mm) to boulders (>256 mm) based upon the Wentworth scale.

[1]Planetary Science Institute, Tucson, Arizona, USA.
[2]Space Science Institute, Boulder, Colorado, USA.
[3]Astrogeology Science Center, U.S. Geological Survey, Flagstaff, Arizona, USA.
[4]Institut für Anorganische Chemie und Analytische Chemie, Johannes Gutenberg-Universität, Mainz, Germany.
[5]Department of Hydrology, University of Bayreuth, Bayreuth, Germany.
[6]Center for Applied Geoscience, Eberhard Karls University of Tübingen, Tubingen, Germany.
[7]Department of Earth and Planetary Sciences, Washington University in St. Louis, St. Louis, Missouri, USA.
[8]Department of Physics, University of Guelph, Guelph, Ontario, Canada.
[9]Department of Astronomy, Cornell University, Ithaca, New York, USA.
[10]NASA Marshall Space Flight Center, Huntsville, Alabama, USA.
[11]Department of Geological Science and Engineering, University of Nevada, Reno, Nevada, USA.
[12]Department of Geological Sciences, Brown University, Providence, Rhode Island, USA.
[13]Mars Space Flight Facility, Arizona State University, Tempe, Arizona, USA.

0148-0227/10/2010JE003660

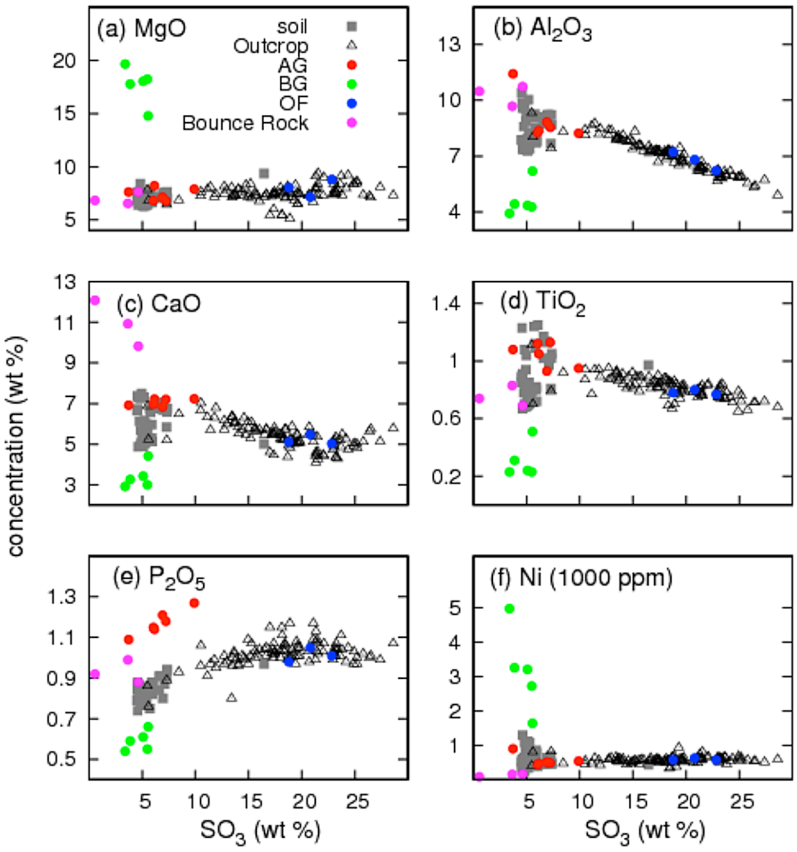

Figure 1. Composition of rock fragments compared to Meridiani outcrop and soil. Outcrop fragments (OF) are indistinguishable from other outcrop rocks; Barberton group cobbles (BG) are clearly different from any other material, and Arkansas group cobbles (AG) appear compositionally close to soil for a number of elements. All three APXS spots on Bounce Rock are plotted.

[3] There are several proposed hypotheses for the origin of the rock fragments at Meridiani [*Jolliff et al.*, 2006; *Fleischer et al.*, 2010b]: (1) fragments of meteorites, (2) resistant material eroded from the outcrop, (3) erosional remnants of a layer that once existed above or is currently located below the present outcrops, (4) fragments of impact ejecta, and (5) impact breccias derived from the outcrop and perhaps mixed with underlying strata. It should be noted that these models are not mutually exclusive.

[4] In general, the rock fragments can be divided into three groups based upon their mineralogy (Figure 1) [*Fleischer et al.*, 2010b]: (1) outcrop fragments, including Lion Stone and Russet, that have the same compositions as the light-toned sulfate outcrop rocks [*Clark et al.*, 2005; *McLennan et al.*, 2005]; (2) meteorite candidates, including Barberton, Santa Catarina, Santorini, and Kasos, which have high Ni contents and the presence of kamacite and troilite and Heat Shield Rock and Block Island, which are iron-nickel meteorites [*Schröder et al.*, 2008; J. W. Ashley et al., Evidence for mechanical and chemical alteration of iron-nickel meteorites on Mars - Process insights for Meridiani Planum, submitted to *Journal of Geophysical Research*, 2010]; and (3) impact fragments, including Bounce Rock, Arkansas, Perseverance, Antistasi, Joseph McCoy, Haiwassee, Tilos, Kos, and Rhodes. Bounce Rock has a basaltic composition similar to the shergottite meteorite EETA79001 [*Klingelhöfer et al.*, 2004; *Rieder et al.*, 2004; *Squyres et al.*, 2006]. The other impact fragments have compositions intermediate between sulfate-rich outcrop and basaltic soil, consistent with impact melt. They could also represent a layer at depth or from somewhere else on Mars that has been mixed and brought to the surface as impact ejecta [*Fleischer et al.*, 2010b].

[5] Here we report on individual rocks in order of the sols they were examined by rover instruments. There are two cobbles (Joseph McCoy and Haiwassee) that were analyzed by APXS and MB but the cobbles could not be confidently identified in the Pancam scene among dozens of similar looking cobbles. However, these two cobbles have a geochemistry similar to several other cobbles (Arkansas, Perseverance, and Antistasi) [*Fleischer et al.*, 2010b] where Pancam spectra were acquired.

2. Data Sets and Analysis Methods

[6] The Pancam multispectral camera on the Opportunity rover acquired the main data set discussed in this paper. Pancam consists of two cameras mounted 1.5 m above the ground on a mast to provide stereo separation [*Bell et al.*, 2003]. Each camera has an eight-position filter wheel with 13 filters covering 11 unique visible/near-infrared (VNIR) wavelengths. Table 1 lists the 13 filter positions. All anal-

Table 1. Pancam Band Names and Centers

Band	Center (nm)
L2	753
L3	673
L4	601
L5	535
L6	482
L7	432
R1	436
R2	754
R3	803
R4	864
R5	904
R6	934
R7	1009

yses conducted in this investigation used data sets that were acquired using all 13 of these bands.

[7] Spectra from regions of interest (rectangles that encompassed between 10 and 100 pixels) were collected manually from common areas in each camera. The spectra were then scaled such that they matched at the L2 and R2 channels (centered at 753 and 754 nm, respectively). The standard deviation shown in the spectral plots represents the pixels that have been averaged together to form the spectra, but do not represent instrumental error. A calibration target was also acquired for each multispectral image and used in conjunction with prelaunch calibration information to convert the raw image data to calibrated radiance and then to radiance factor (I/F, where I is the measured radiance and F is the incident solar irradiance) [*Bell et al.*, 2003, 2006]. The data was then converted to relative reflectance (R*, defined as I/F divided by the cosine of the incidence angle [*Reid et al.*, 1999; *Bell et al.*, 2006]) using the solar incidence angle for each scene. Calibration of the images to R* results in a first-order correction of the diffuse sky illumination for surfaces at or near the same solar incidence angle as the calibration target. Absolute reflectance levels of these data are believed to be accurate to within ~10% for the shorter wavelengths and slightly less (better) at longer wavelengths [*Bell et al.*, 2006]. Data were typically compressed on the rover before downlink and effects from the compression are estimated to cause < 1% error on the radiometric precision [*Bell et al.*, 2006]. More details concerning the calibration and sources of error of the Pancam data can be found in the work of *Bell et al.* [2006], *Farrand et al.* [2007, 2008], and *Johnson et al.* [2006].

[8] Simple three band color composites and decorrelation stretches have been produced for each of the cobbles. The three band color composites consist of the L2, L5, L6 (L256) bands. In order to increase the subtle differences in color, we applied decorrelation stretches to the bands [*Gillespie et al.*, 1986; *Farrand et al.*, 2007]. The color representations in the decorrelation stretch images depend upon the materials and variations of spectra within the scene so the colors only apply to a given scene. Decorrelation stretch images consist of the L2, L5, L7 (L257) or R2, R6, R7 (R267) bands.

[9] Most soils on the Meridiani plains and within impact craters have millimeter size spherules informally referred to as "blueberries." The hematite-rich spherules are postulated

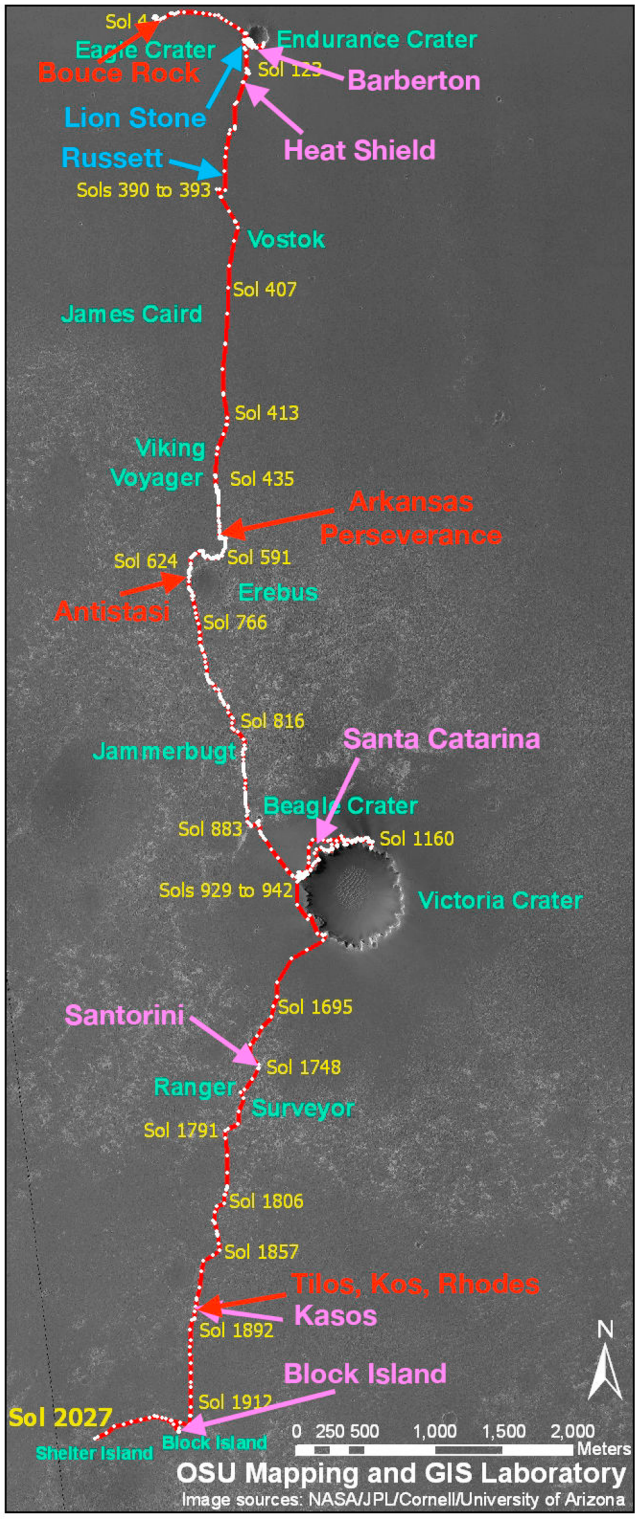

Figure 2. Traverse of Opportunity rover through sol 2027. Rock fragments analyzed in this study are shown along the traverse path, with the colors representing the type of rock (blue for outcrop fragments, pink for meteorite fragments, and red for impact fragments). Informal names for impact craters are also shown.

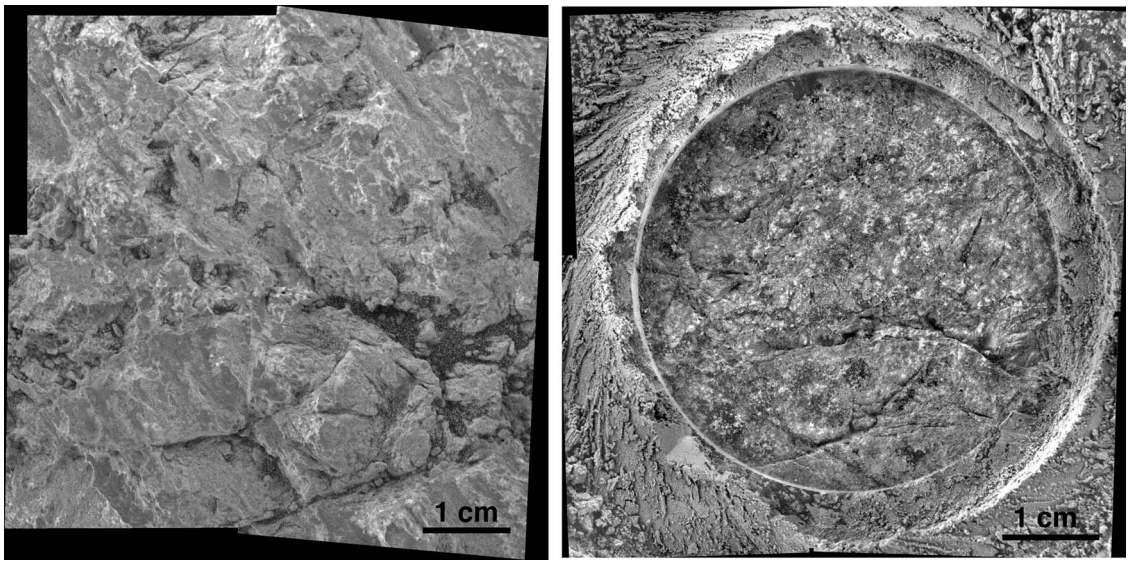

Figure 3. MI mosaic of Bounce Rock acquired (left) pre-RAT and (right) post-RAT.

to have formed by secondary alteration of the sulfate-rich outcrop as water permeated through the rocks and produced concretions [*McLennan et al.*, 2005]. Proposed origins for the exposed outcrop at the landing site include impact surge deposits [*Knauth et al.*, 2005], a basaltic pyroclastic deposit subsequently altered through reaction with an aqueous sulphuric acid solution [*McCollom and Hynek*, 2005], and erosion and redistribution of sand grains that originally were derived by chemical weathering of olivine basalt in aqueous solutions of sulfuric acid, forming sulfate salts that accumulated with fine grained silicates [*Squyres et al.*, 2004, 2006; *Grotzinger et al.*, 2005]. The spherules are more resistant to erosion and collect as a soil lag on the surface as the friable outcrop is eroded and removed by the wind.

[10] In order to explore possible illumination effects for Pancam images of the rock fragments, we have also acquired spectra of blueberries and outcrop within any given scene if they are visible and resolvable. Thus far, no chemical variations have been identified in the blueberries throughout the landing site, although their small size (~1–4 mm diameter) makes it impossible to acquire an in situ measurement of individual blueberries and thus an average is made for a cluster of spherules that fill the field of view for the IDD instruments (~1.5 cm for MB and ~2.5 cm for APXS). We assume for this study that all blueberries share the same chemistry, and consequently, Pancam spectra for blueberries should not reflect any intrinsic mineralogic differences. We do, however, expect to see different amounts of air fall dust on individual blueberries, specular reflections, and lighting geometry variations that would affect the spectra acquired for blueberries depending upon the scene. Indeed, by comparing spectral variability of blueberries within a given scene, we can better understand variations in Pancam spectra of the rock fragments. In general, each spectrum

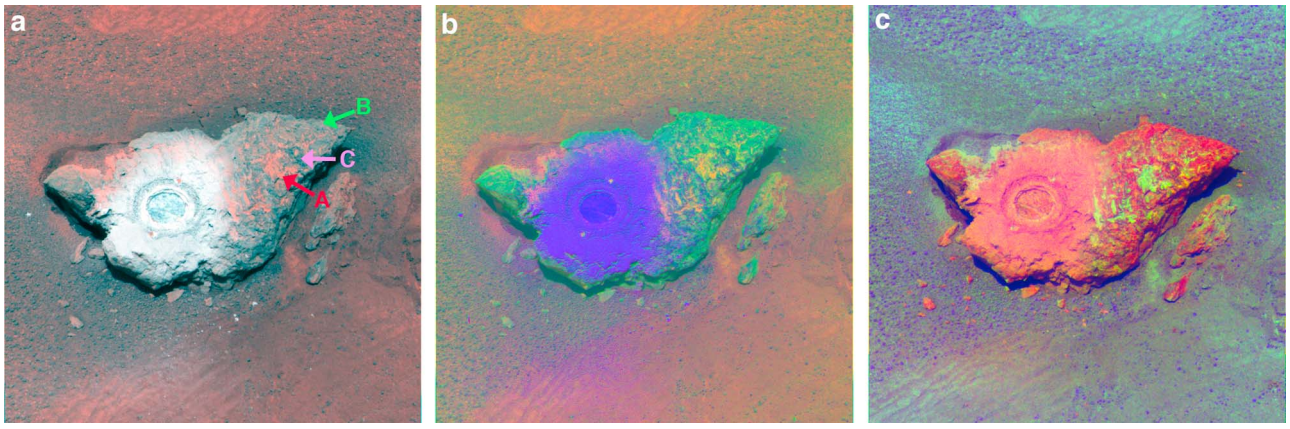

Figure 4. (a) Pancam color composite with L2 in red, L5 in green, and L6 in blue of Bounce Rock taken after the RAT hole was made. Locations A, B, and C are where spectra were extracted and shown in Figure 5. (b) Decorrelation stretch with L2 in red, L5 in green, and L7 in blue. (c) Decorrelation stretch with R2 in red, R6 in green, and R7 in blue.

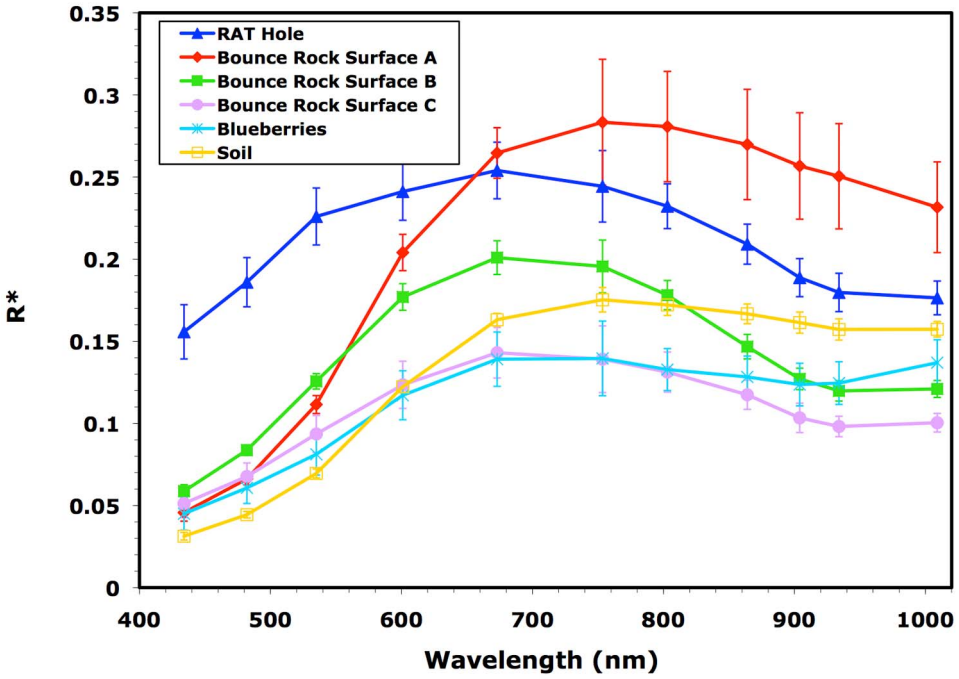

Figure 5. Spectra from Bounce Rock with surfaces A, B, and C shown in Figure 4. Surface A is characteristic of dust, while the RAT hole and surfaces B and C are consistent with pyroxene. The spectrum for the blueberries has an absorption in the NIR with a strong upturn between 934 and 1009 nm.

shown for blueberries represents an average of between 3 and 10 blueberries from the same scene.

[11] Outcrop spectra are more variable owing to subtle chemical, alteration, and other surficial processes that have affected the outcrop over time. *Farrand et al.* [2007] noted that Meridiani outcrop can be divided into two spectral classes: (1) HFS (High Four hundred eighty-two to 535 nm Slope): more oxidized, lighter-toned and buff colored in L256 composites and (2) LFS (Low Four hundred eighty-two to 535 nm Slope): less oxidized, darker-toned and purple colored in L256 composites. Consequently, we expect to observe a larger degree of spectral heterogeneity for outcrop exposures compared to blueberries.

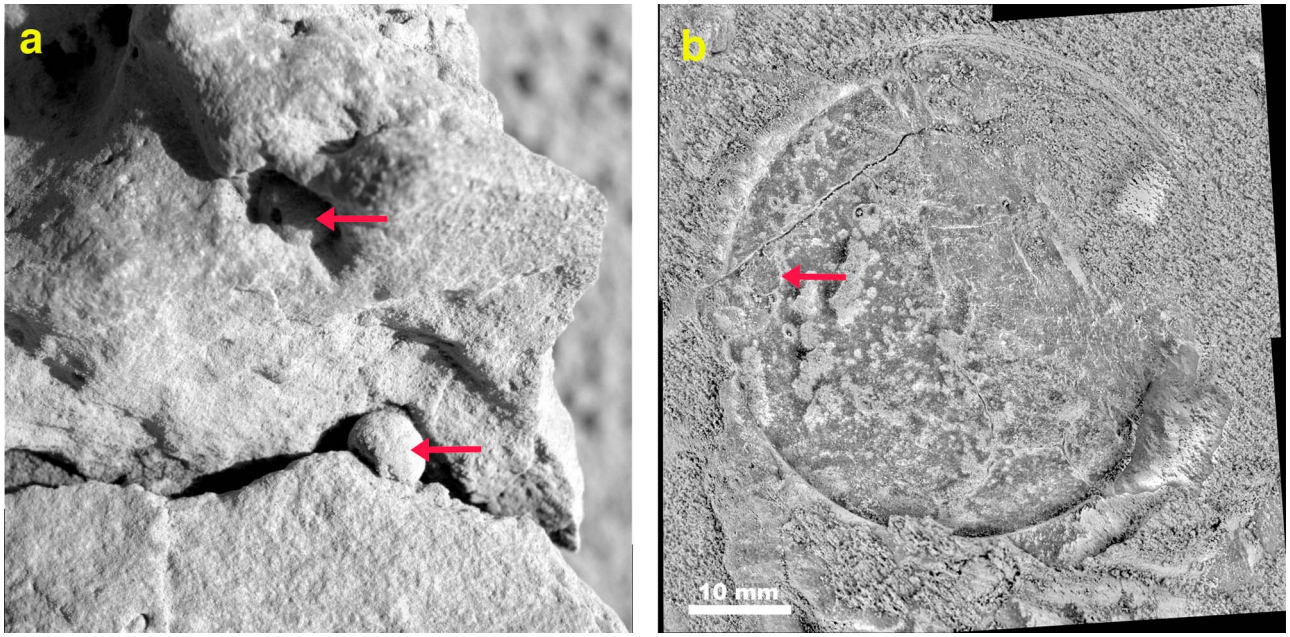

Figure 6. (a) MI image of Lion Stone surface. Embedded blueberries are shown by red arrows. (b) MI mosaic of RAT hole in Lion Stone with embedded blueberry shown by red arrow.

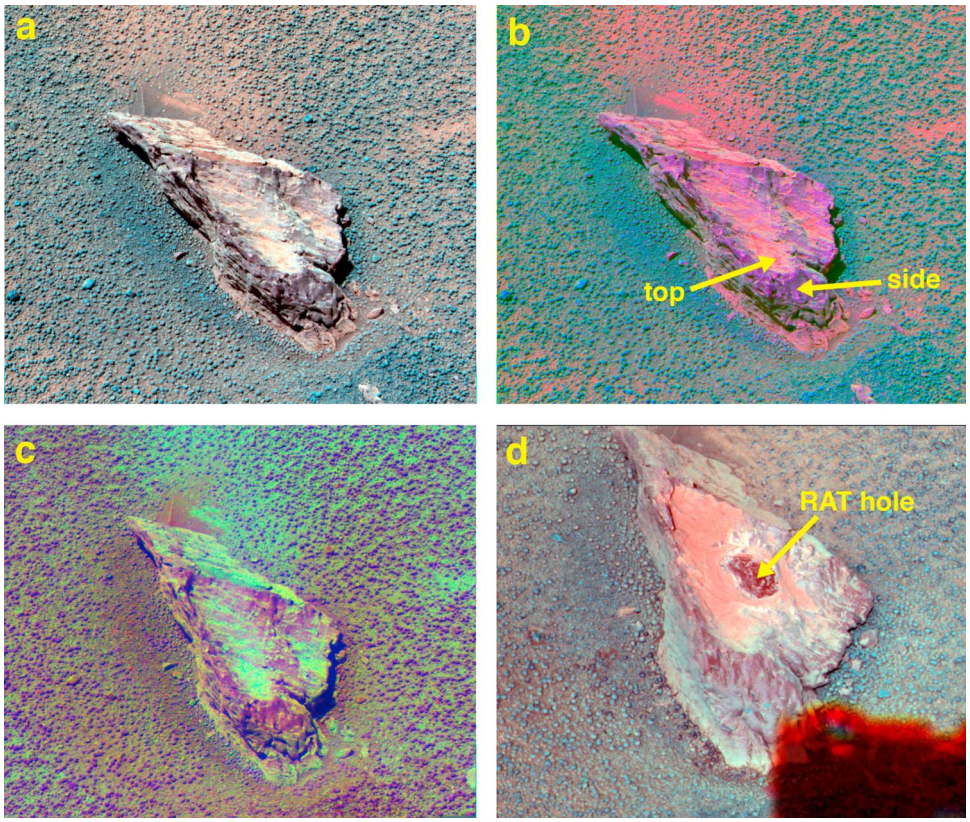

Figure 7. (a) L2, L5, and L6 composite of Lion Stone. The top surface appears dusty. Blueberries (blue spherules) can be seen in the soils around Lion Stone. (b) L257 decorrelation stretch image. (c) R267 decorrelation stretch image. (d) L256 composite after grinding the RAT hole.

[12] We also use data acquired by several of the in situ instruments on the robotic arm, including: Microscopic Imager (MI) with a resolution of 30 μm/pixel or images 31x31 mm across [*Herkenhoff et al.*, 2003, 2008]; APXS for elemental composition [*Rieder et al.*, 2003]; and MB for Fe oxidation states and Fe-bearing mineral measurements [*Klingelhöfer et al.*, 2003]. The geochemistry measurements of the rock fragments are not a focus of this paper, however, and have been discussed in other publications [e.g., *Schröder et al.*, 2008; *Fleischer et al.*, 2010b; *Schröder et al.*, 2010]. Instead, we focus on Pancam spectral analyses and comparison of the VNIR spectral interpretations of mineralogy to measurements made by the in situ instruments.

[13] In addition to spectral analyses, we have also used Pancam data in combination with MI images to analyze the shape, roundness, and textures of the rock fragments [*Yingst et al.*, 2008]. The shape of a rock can provide important insight about formation and modification. Sphericity is the ratio that determines how close a particle approximates a sphere, with 1.0 representing a perfect sphere. Roundness is a measure of the sharpness of grain corners. Together, these physical attributes and spectral results have been used to infer likely origins and alteration mechanisms for each rock fragment. Note that in most cases, measurements of roundness and sphericity are based on images acquired from a single viewpoint, and the unseen portions of the rock may have exhibited a different surface shape that could have influenced the overall roundness/sphericity calculations had they been observed.

3. Data Analysis of Individual Rock Fragments

[14] In this section we describe analyses conducted on each rock fragment by the rover instruments. The results from MI, APXS and MB are discussed along with Pancam spectra. A comparison of the spectral properties for all the rocks is described in section 4.

3.1. Bounce Rock (Sols 66–70)

[15] After egress from Eagle Crater, Opportunity analyzed an unusual loose rock about 20 m beyond the crater rim (Figure 2). The rock had been pushed slightly into the ground by the impact from one of the lander inflatable airbags and was hence dubbed "Bounce Rock." The rock is ~40 cm long and irregular in shape with a sphericity of 0.62 and roundness of 0.53 (qualitative roundness is angular). The results from miniThermal Emission Spectrometer (miniTES), APXS and MB analyses indicate the rock is dominated by pyroxene, consistent with a basaltic composition similar to the shergottite meteorite EETA79001 [*Klingelhöfer et al.*, 2004; *Rieder et al.*, 2004; *Christensen et al.*, 2004; *Squyres et al.*, 2006; *Zipfel et al.*, 2010]. The rock is most likely an impact fragment not locally derived but potentially from a crater 75 km to the southwest [*Squyres et al.*, 2004].

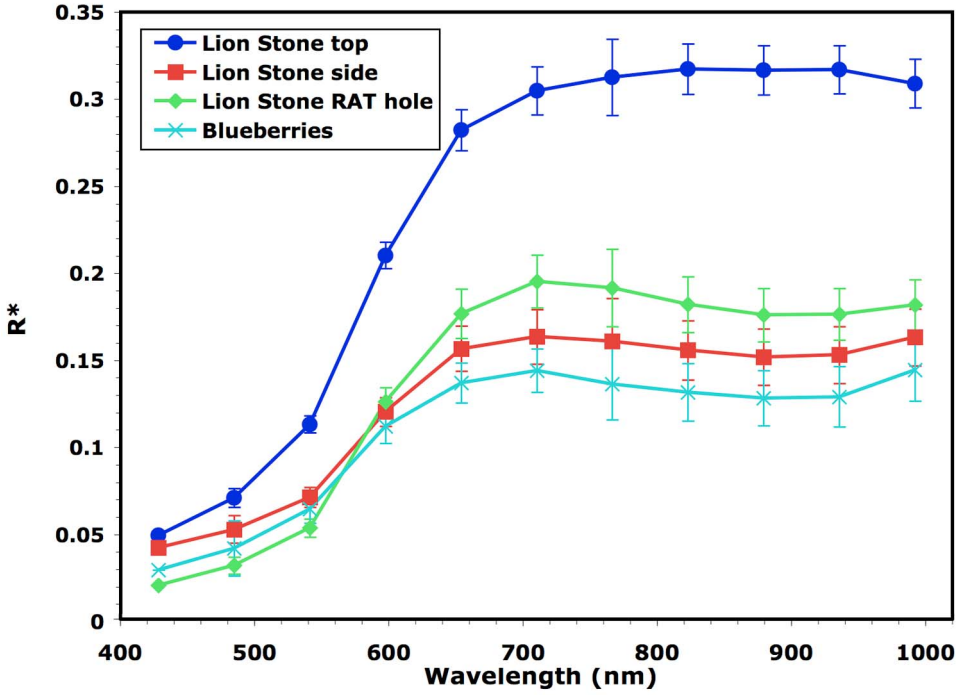

Figure 8. Spectra from Lion Stone. The sides and RAT hole are different from the upper surface of the rock, perhaps due to weathering rinds and dust coatings on the flatter top surface. The spectrum for the blueberries has a strong upturn between 934 and 1009 nm, characteristic of the hematite-rich composition of the spherules.

[16] Mosaics of MI images taken before and after use of the RAT are shown in Figure 3. The RAT produces ~4.5 cm diameter holes that are typically several millimeters deep [*Gorevan et al.*, 2003]. None of the MI images show convincing evidence for phenocrysts. The pre-RAT surface shows fractures and small pits, many of which are filled in with sand and millimeter size pebbles. The surface displays small amounts of brightness variations that can be attributed to variable degrees of dust. The RAT hole exposes small fractures but no significant heterogeneities in brightness, roughness, or evidence of crystals.

[17] Pancam false color images of Bounce Rock are shown in Figure 4. The RAT hole created a large amount of fine debris that obscured the original surface of the rock. In the composite and decorrelation stretches, color variations can be seen in the right portion of Bounce Rock where there is no contamination by RAT hole cuttings. Spectra were acquired from three locations (Figure 4a) on the surface of Bounce Rock that were distinguishable in the color images. In addition, a spectrum of spherule-free soil and a spectrum that represents the average of several blueberries in the soil are shown in Figure 5. As noted by others [e.g., *Weitz et al.*, 2006] the blueberries have an upturn inflection between the 934 and 1009 nm bands that is characteristic of hematite. Location A on Bounce Rock has a spectrum that is similar to dust (Figure 5). In contrast, spectra from locations B and C have long wavelength absorptions that could match pyroxene or olivine. The RAT hole spectrum has the same long wavelength absorption but not as steep a slope in the visible, probably due to lack of dust. *Bell et al.* [2004] interpreted the presence of pyroxene or olivine within the rock based upon similar Pancam spectra of Bounce Rock. Consequently, the Pancam spectra of Bounce Rock are consistent with the basaltic composition determined by APXS and MB.

3.2. Lion Stone (Sols 106–108)

[18] Before entering Endurance crater, Opportunity analyzed a 35 cm long rock dubbed Lion Stone. The rock is elongated and has thin bedding with a sphericity of 0.63 and roundness of 0.11 (qualitative roundness is very angular). It does not appear to be loose lying on the surface but rather connects to underlying partially buried outcrop. Lion Stone was analyzed before and after use of the RAT grind. MI images show a surface similar to that seen in outcrop with embedded blueberries and vugs (Figure 6a). A fracture and blueberry can be seen in the RAT hole MI mosaic image (Figure 6b).

[19] APXS and MB measurements indicate the composition is dominated by silica and sulfur and sulfate minerals. Both the pre- and post-RAT chemical measurements are similar to those of typical outcrop exposures. Hence, the rock is either a high-standing outcrop or proximal crater ejecta from the outcrop.

[20] Figure 7 shows the pre- and post-RAT Pancam images of Lion Stone. Much of the top surface has a different color than the remainder of the rock. The darker RAT hole represents a dust-free and fresher surface (Figure 7d) and its spectrum is similar to the side of the rock (Figure 8). Spectra for blueberries embedded within the rock are similar to spherules adjacent to Bounce Rock on the ground. When

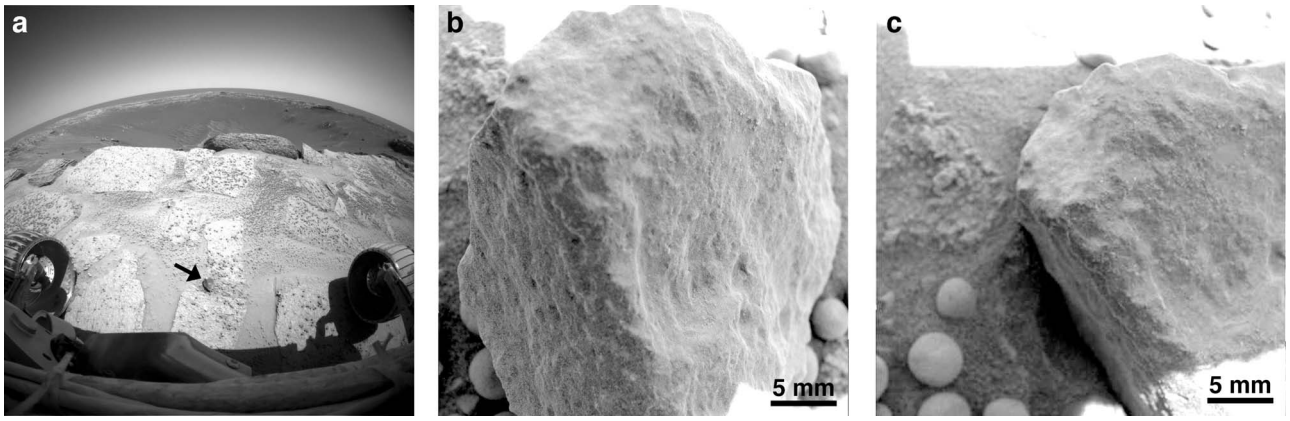

Figure 9. (a) Front Hazard Camera showing Barberton on the edge of Endurance crater, seen in the background. (b) MI image of Barberton. (c) MI image of Barberton and blueberries.

compared to other outcrop spectra from *Farrand et al.* [2008], the RAT hole and side spectra for Lion Stone closely match outcrop with steeper faces and at the distal portions of layers (LFS spectral class). In contrast, the upper surface of the rock has spectra comparable to the HFS outcrops, which are typically buff colored with flatter surfaces [*Farrand et al.*, 2008]. Based upon these Pancam results, it would be difficult to uniquely determine the mineralogy of the rock (i.e., that the rock is dominated by silica and sulfates) without the geochemistry measurements.

3.3. Barberton (Sols 121–123)

[21] Barberton is a ~3 cm pebble on the rim of Endurance crater (Figure 9a). In MI images (Figures 9b and 9c), the pebble has an indistinct surface texture that could result from dust accumulation. Its shape is angular with flat facets intersecting at sharp angles. No layering or crystals are visible. The sphericity is 0.89 and the roundness is 0.74 (qualitative roundness is subangular).

[22] APXS measurements show high Ni, Mg and low Al, Ca contents (Figure 1), although the pebble was small enough that it probably did not completely fill the field of view. MB measurements are dominated by pyroxene and olivine, with evidence for metallic iron in the form of kamacite and the sulfide troilite, characteristic of meteorites [*Schröder et al.*, 2008]. Comparison to known meteorites suggests a chemical similarity to mesosiderite silicate clasts [*Schröder et al.*, 2008]. Mesosiderites are stony irons and relatively rare on Earth. Barberton's proximity to Endurance crater suggests that it could represent a piece of the impactor that created the crater.

[23] Pancam false color and decorrelation stretch images of Barberton are shown in Figure 10. The pebble is situated on a flat outcrop exposure and surrounded by loose blueberries. The MB imprint into a nearby soil is also visible in the Pancam scene. The spectrum for the outcrop (Figure 11) is consistent with other outcrop exposures seen at Meridiani. The spectrum for blueberries is atypical, with two apparent absorptions at 754 nm and 904 nm compared to the typical one absorption seen at 904 nm in other Pancam scenes, although the error bars are very large. The blueberries spectrum does have the characteristic strong upturn between the 934 and 1009 nm filters.

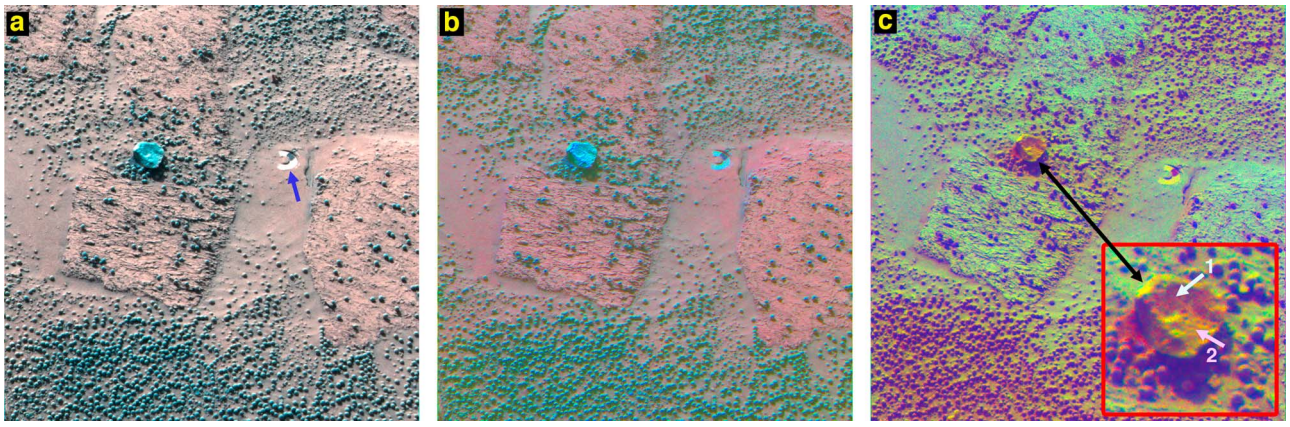

Figure 10. Pancam scene of Barberton and adjacent soils. (a) False color composite with Barberton (blue rock fragment) and MB imprint into fine soil (purple arrow). (b) L257 decorrelation stretch and (c) R267 decorrelation stretch with blowup of Barberton showing surfaces where spectra were extracted (locations 1 and 2).

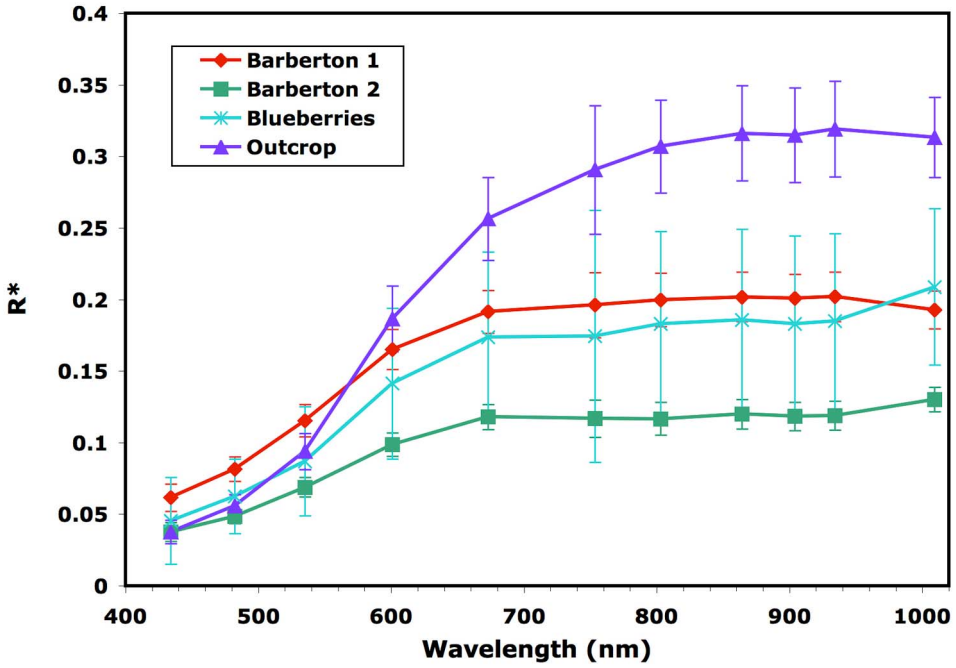

Figure 11. Spectra of Barberton and other nearby materials.

[24] In the decorrelation image (Figure 10c), Barberton exhibits some spectral variation. Extracted spectra from two locations on Barberton indicate these variations could be attributed to different amounts of atmospheric or outcrop-derived dust, as indicated by the larger reflectance and absorption at 1009 nm band in Barberton 1. Barberton 2 has two apparent absorptions, one around 803 nm and the other around 900 nm. Based upon the Pancam spectra of Barberton, we cannot adequately determine mineralogy nor confirm whether it is a stony meteorite. However, Barberton's distinct spectra from outcrop material and its location along the rim of Endurance would evoke a nonlocal, and therefore possibly meteoritic, origin.

3.4. Heat Shield Rock (Sols 347–352)

[25] The rover analyzed a 31 cm size boulder that was only a few meters from the heat shield used during descent of the lander. The MER team dubbed it "Heat Shield Rock," although it is officially recognized as a meteorite with the name "Meridiani Planum." The rock has a pitted surface

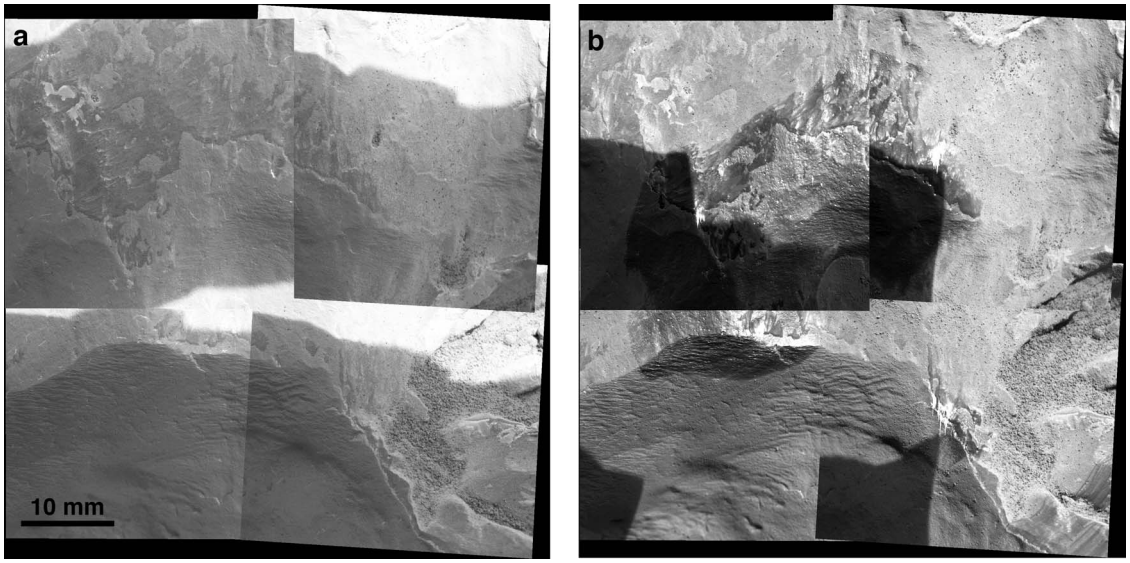

Figure 12. MI mosaics of Heat Shield Rock acquired (a) pre-RAT and (b) post-RAT brush.

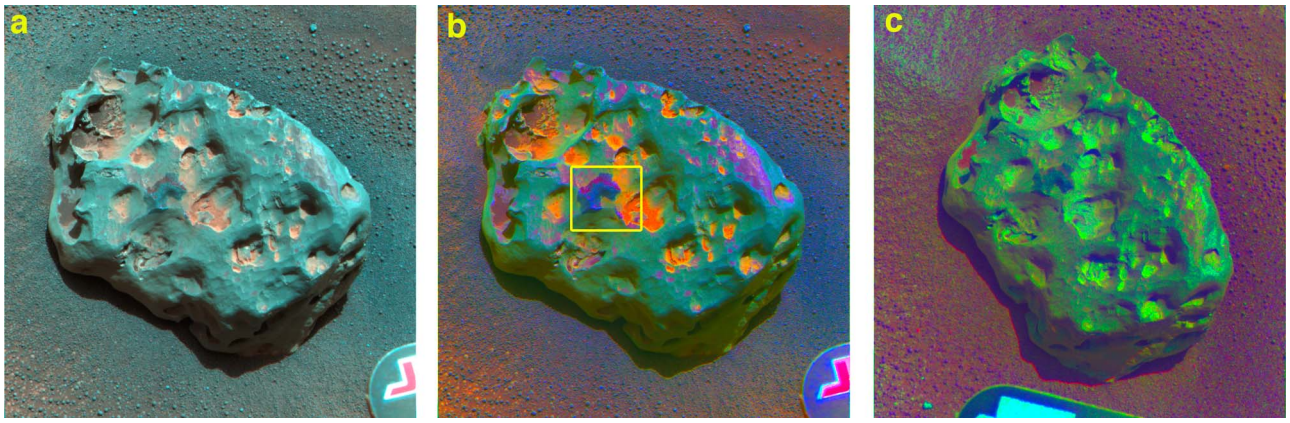

Figure 13. Pancam images of Heat Shield Rock taken post-RAT brush. (a) L256 color composite. (b) L257 decorrelation stretch. Yellow box identifies blowup shown in Figure 14. (c) R267 decorrelation stretch. Note that a portion of the rover deck is visible in the bottom of each image.

with quasi-specular reflections (Figure 12) and hollows, some of which resemble regmaglypts (J. W. Ashley et al., submitted manuscript, 2010), giving it a distinct appearance from the typical rocks seen along the Meridiani plains by Opportunity. The sphericity is 0.79 and roundness is 0.198 (qualitative roundness is subround). Heat Shield Rock was analyzed by the IDD instruments both pre- and post-RAT brush.

[26] Initial remote sensing by MiniTES indicated the rock was metallic [*Schröder et al.*, 2008; *Ruff et al.*, 2008]. The composition of the rock is dominated by 93% Fe with 7% nickel as measured by the APXS [*Schröder et al.*, 2008] and the mineral kamacite was determined on the basis of the Fe/Ni ratio using the MB [*Morris et al.*, 2006; *Fleischer et al.*, 2010a]. Based upon these compositions, the rock is classified as an IAB complex iron meteorite [*Schröder et al.*, 2008].

[27] Pancam images, especially the L257 decorrelation stretch image, show heterogeneities on the surface of the rock (Figure 13). Spectra extracted from the brushed region (Figure 14) indicate that the purple material has a deeper 535 nm band most likely attributable to more oxidation relative to the bluer material [*Schröder et al.*, 2008]. MI images reveal the pits in the rock are filled with small particles. A Pancam spectrum from one of the pits (Figure 14, Heat Shield Pit) is characteristic of air fall or outcrop-derived dust. Most of the surface of Heat Shield Rock has a broad but shallow absorption in the NIR region. *Schröder et al.* [2008] determined that the brushed surface spectrum is similar to the iron meteorite Canyon Diablo laboratory

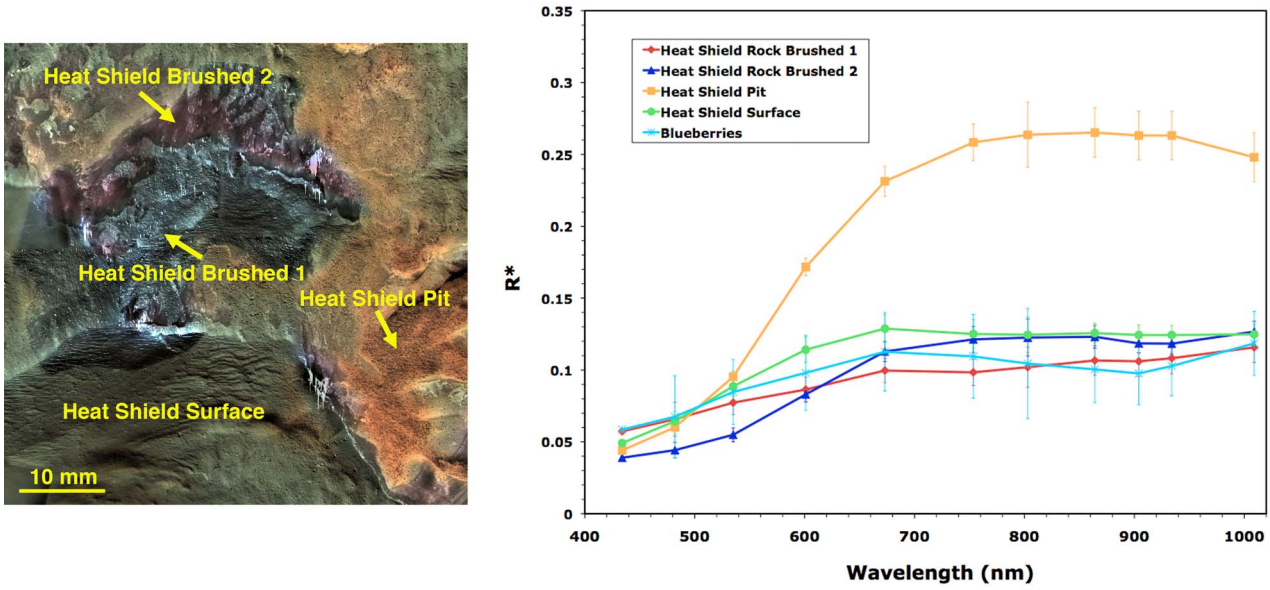

Figure 14. (left) Pancam decorrelation stretch L257 overlain on MI mosaic. The brushed area has two distinct surfaces (brushed 1 in blue and brushed 2 in purple). The unbrushed surface looks green, while a pit appears orange and covered by fine particles. (right) Associated Pancam spectra of these same regions as well as blueberries that are found adjacent to Heat Shield Rock.

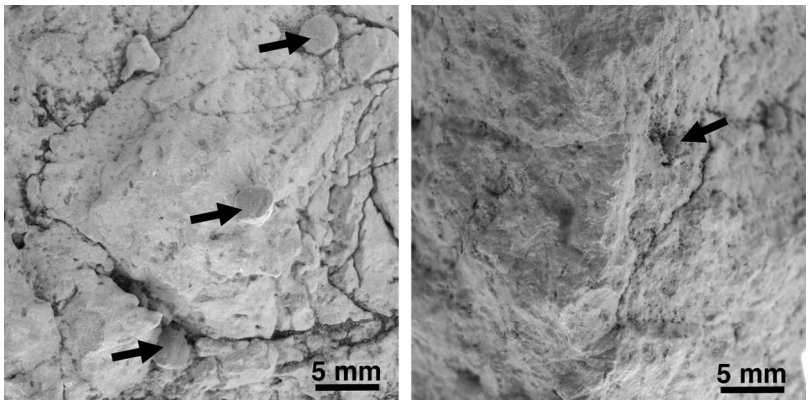

Figure 15. MI images of Russett reveal a cracked surface with embedded blueberries (black arrows).

spectrum. Hence, the Pancam spectra when combined with morphological features, thermal infrared spectra [*Ruff et al.*, 2008], and chemistry of Heat Shield Rock, can be used to infer an iron meteorite.

3.5. Russett (Sols 381–382)

[28] Russett is an unusual shaped rock about 10 cm long with a bumpy, irregular profile. Its sphericity is 0.75 and the roundness value is 0.18 (qualitative roundness is very angular). Because of its odd shape and location along the rippled plains away from outcrop exposures, it was initially thought that the rock could be of impact origin. Closer inspection of the rock showed embedded blueberries (Figure 15), indicating it was probably derived as an impact fragment from outcrop material. Its composition is similar to other Meridiani outcrops with low Fe and high Mg, Si, and S, consistent with the rock being a fragment of outcrop material. A local impact event that displaced a small fragment of outcrop is the most plausible origin for Russett.

[29] Pancam images reveal slight heterogeneities in color across the surface of Russett (Figure 16). The color variations could reflect different amounts of coatings along surfaces rather than intrinsic mineralogic variability in the rock. A spectrum for Russett (Figure 17) has a steep upward slope in the visible and an absorption at the longer wavelengths around 900 nm. This spectrum is also characteristic of outcrop exposures, although Pancam spectra of many outcrop exposures throughout the landing site show some variability [*Farrand et al.*, 2007]. Spectrally, Russett is similar to the purple-colored LFS unit identified by *Farrand et al.* [2007] for steeper-faced outcrop surfaces in the Burns Formation. Spectra for several blueberries in the scene have the characteristic strong upturn between 953 and 1009 nm, as well as the broad absorption around 900 nm that is typical of the hematite-rich spherules.

3.6. Arkansas and Perseverance (Sols 551–554)

[30] Arkansas and Perseverance are two of dozens of cobbles clustered together along small patches of outcrop just north of Erebus crater (Figure 2). The 9.4 cm long Arkansas shows no evidence of individual grains, although the surface texture has heterogeneities [*Herkenhoff et al.*, 2008]. MI images (Figure 18a) were acquired in shadow so lighting conditions are not ideal for determining brightness and luster. In contrast, sunlit MI images of Perseverance (Figure 18b) reveal a mottled, heterogeneous appearance for

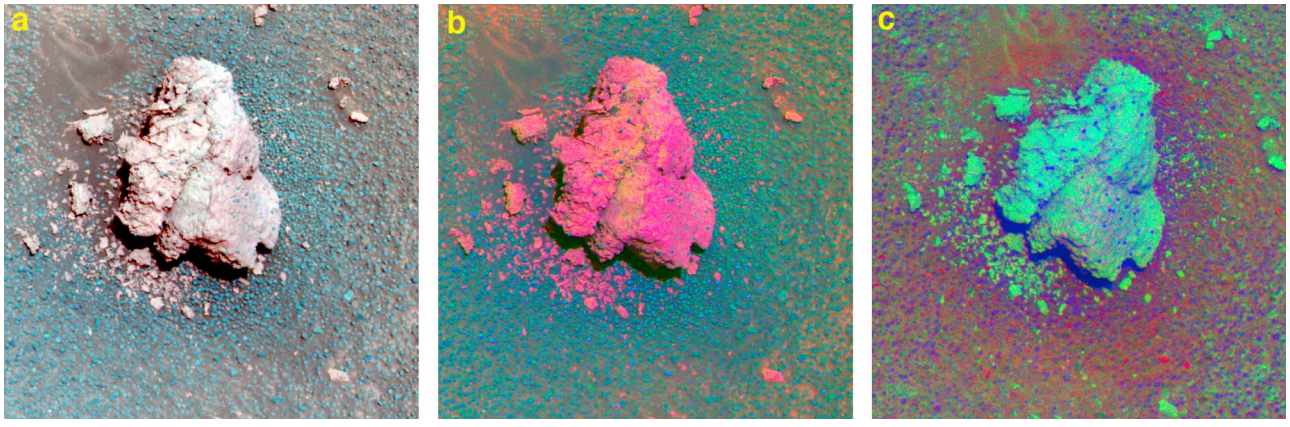

Figure 16. Pancam images of Russett. (a) L256 color composite shows numerous small fragments on the ground that are most likely pieces that broke off of Russett. (b) L257 decorrelation stretch and (c) R267 decorrelation stretch image. There are slight color variations across the rock surface that could result from patchy dust or alteration coatings.

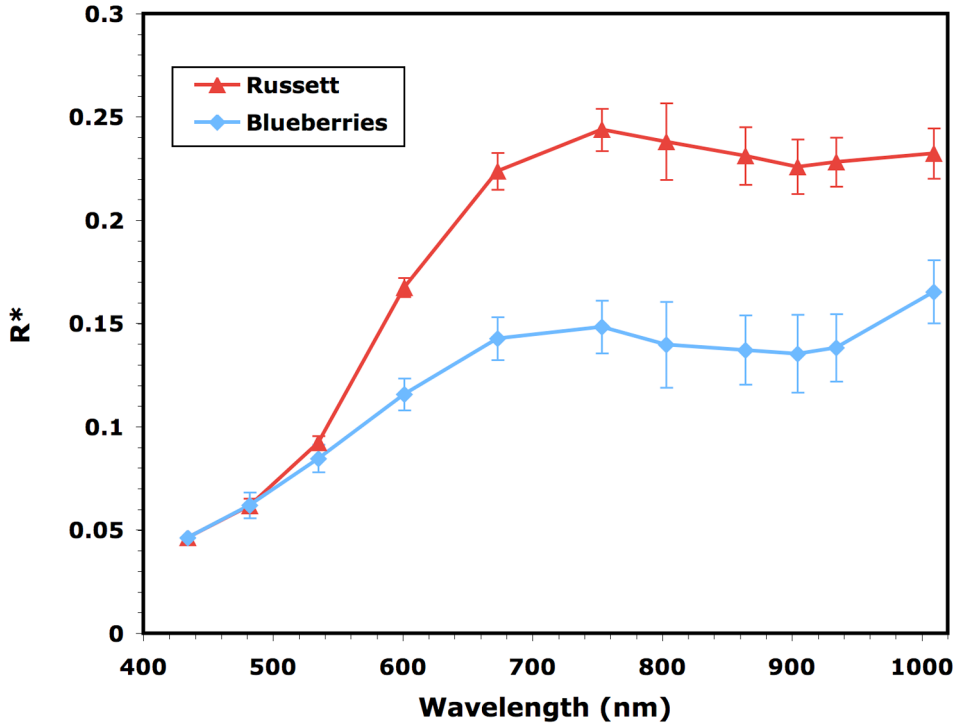

Figure 17. Spectrum of Russett is consistent with other outcrop materials at Meridiani Planum. The blueberries also have a spectrum typical of other hematite-rich spherules seen elsewhere at the site.

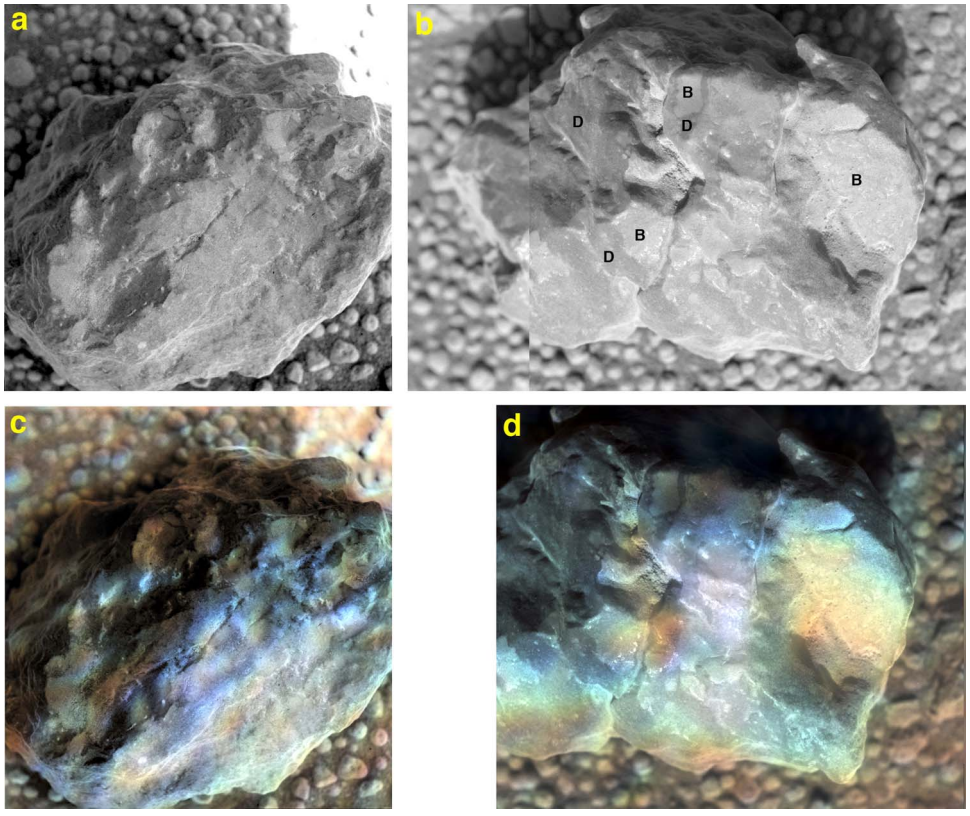

Figure 18. (a) MI image of the 9.4 cm long Arkansas. (b) MI image of the 10.2 cm long Perseverance. Letters denote regions that appear bright (B) and dark (D). (c and d) Pancam L257 color merged with MI images.

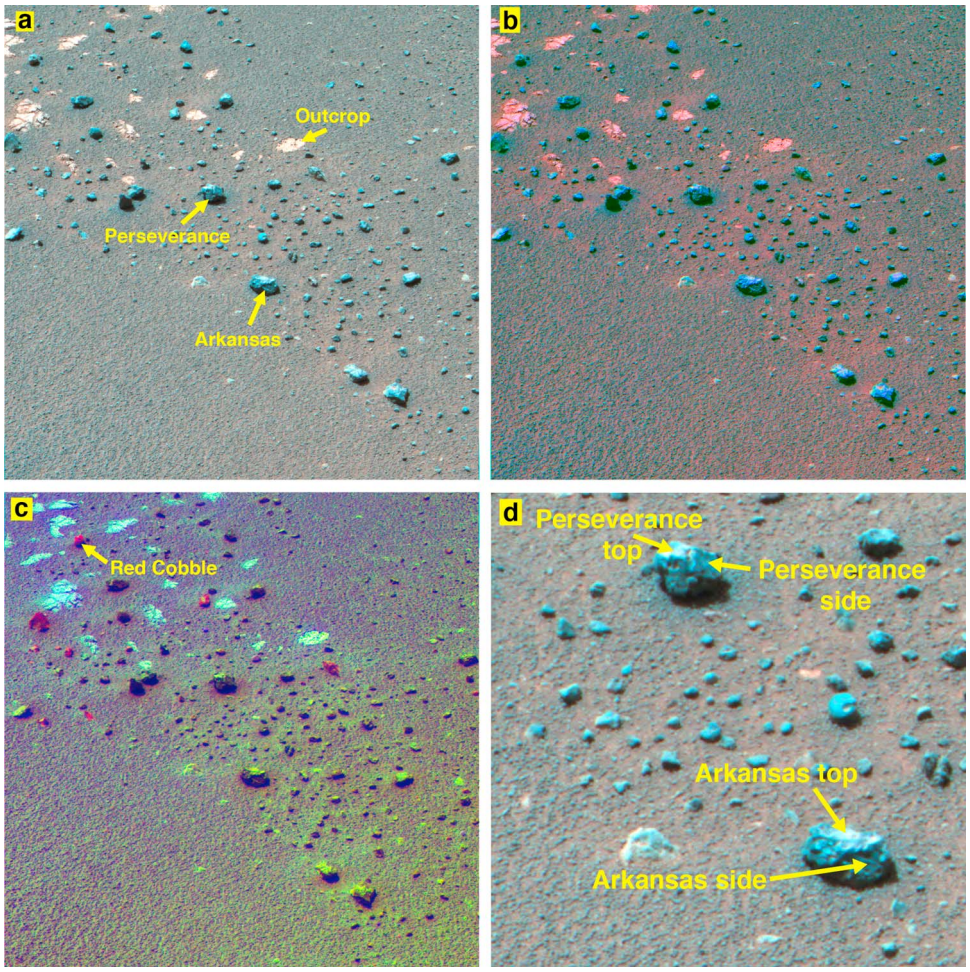

Figure 19. Pancam scene of the cobbles Arkansas and Perseverance. (a) All the cobbles appear blue in this color composite. (b) L257 decorrelation stretch image. (c) R267 decorrelation stretch image reveals color variations between the cobbles. Arkansas and Perseverance appear purple with green top surfaces, while other cobbles appear red. (d) Locations where spectra were extracted.

the 10.2 cm long cobble [*Herkenhoff et al.*, 2008]. Lighter irregular areas 1–20 mm across appear mixed into a darker matrix. Small (<1 mm) dark spots could be basaltic sand and diffuse bright areas in the crevices could represent dust. The textures seen in both cobbles are consistent with breccias. The sphericities are 0.78 and 0.82 and roundness values are 0.12 and 0.37 (angular/subangular for qualitative roundness) for Arkansas and Perseverance, respectively.

[31] The MB mineralogy of Arkansas looks similar to outcrop but with less hematite and no jarosite. In addition, there is no evidence for kamacite or troilite, indicating it is not a meteorite. APXS data indicate relatively high amounts of Al, P and less S than in the outcrop (Figure 1) with a more soil-like composition. Their compositions are similar to rocks and especially soils at the landing site suggesting they either represent outcrop that has been altered (perhaps by impact processes) or they are impact melt derived from mixtures of soil and outcrop found at Meridiani Planum [*Fleischer et al.*, 2010b].

[32] Because the two cobbles are near each other, one Pancam scene was acquired to image both of them simultaneously, as well as several other cobbles in the same location. The soil at this location is covered with blueberries but unfortunately the Pancam resolution is not sufficient to resolve the spherules individually for spectral analysis.

[33] All the cobbles appear blue in the L256 composite and L257 decorrelation stretch images (Figure 19). However, in the R267 decorrelation stretch image, the cobbles show color variations. Arkansas and Perseverance appear similar to the majority of cobbles in the scene with dark purple sides and bright green top surfaces. The top surfaces of several of the cobbles, including Arkansas and Perseverance, have spectra consistent with dust or outcrop-derived materials, including steep slopes in the visible and strong downward slopes between 934 and 1009 nm (Figure 20). However, several cobbles appear red in the R267 decorrelation stretch image. Relative to Arkansas and Perseverance, the red cobbles have a strong absorption around 934 nm and a steeper slope in the visible characteristic of pyroxene (Figure 20). The difference in spectra between red cobbles and Arkansas/Perseverance cobbles could be due to variable amounts of coatings on the surfaces. Alternatively, there could be two different cobble lithologies at this location. Spectrally, the cobbles are all distinct from outcrop materials.

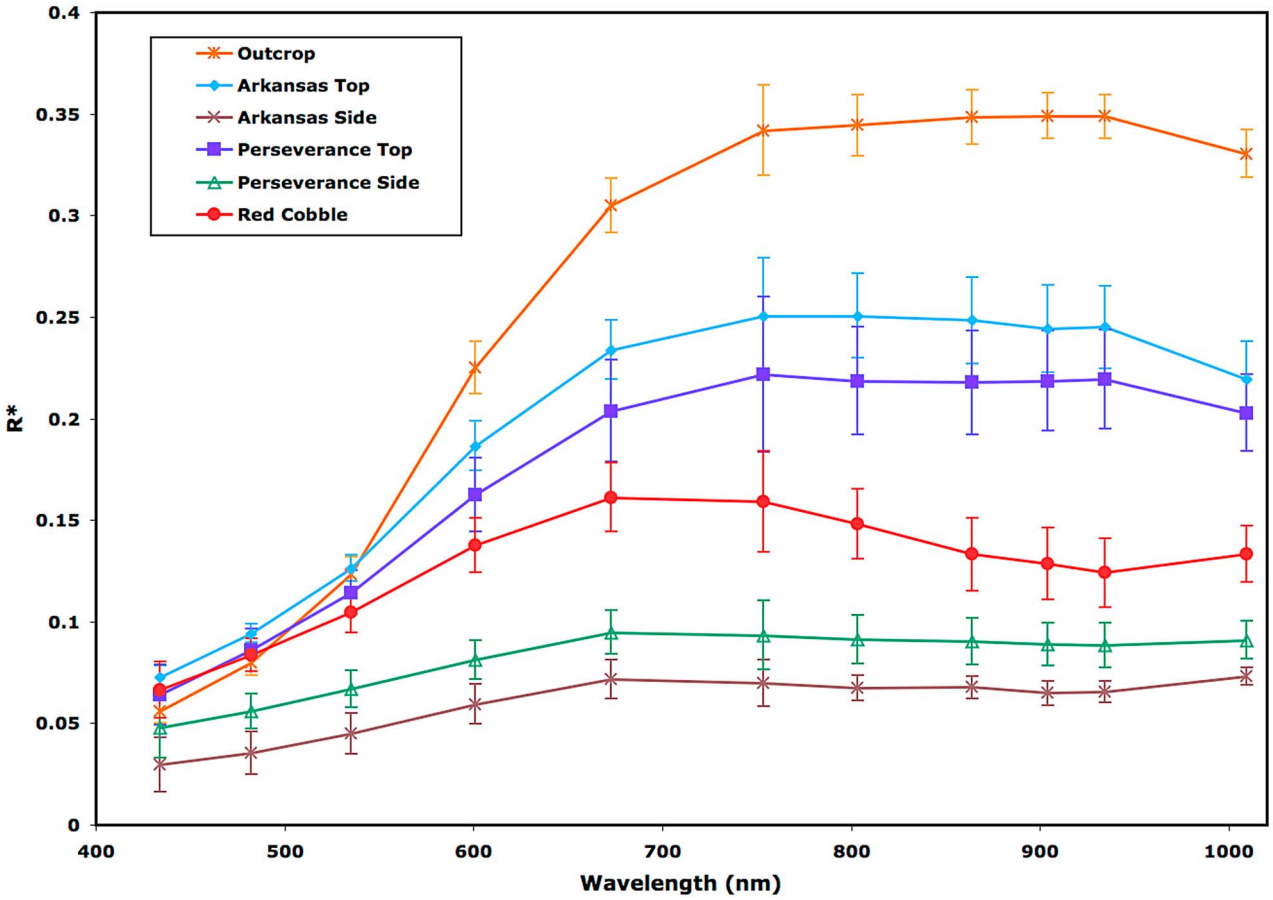

Figure 20. Spectra extracted from various targets, including the cobbles Arkansas and Perseverance. The spectra for the top surfaces of the cobbles are consistent with dust or outcrop-derived coatings. The cobbles that appear red in the R267 decorrelation stretch image have a strong absorption centered around 934 nm relative to the Arkansas and Perseverance types.

3.7. Antistasi (Sols 641–645)

[34] The MI images of the ~10 cm diameter Antistasi were acquired in shadow but the surface shows heterogeneities in brightness with bright spots and rings in a dominantly darker matrix (Figure 21), similar to the appearance of Perseverance. The cobble also has cracks and pits, with some smooth and rounded edges suggesting weathering with time [*Herkenhoff et al.*, 2008]. Bright fines occur along shallow pits and could be collections of dust and other eolian debris. The sphericity is 0.86 and the roundness is 0.065 (qualitative roundness is angular/subangular).

[35] The chemistry of Antistasi is slightly different from Arkansas and Perseverence, with lower amounts of SO_3 and higher Ni contents. Relative to Arkansas, MB measurements detect higher amounts of olivine and pyroxene and lower values of hematite, indicating a larger basaltic contribution [*Fleischer et al.*, 2010b].

[36] Pancam false color images of Antistasi suggest patches of dust atop the rock's surface (Figure 22). Additional color variations in the L257 decorrelation stretch image include green and blue. Spectral variations between these green and blue areas are very subtle. A smaller cobble a few cm to the right of Antistasi has the same spectra, suggesting both cobbles were derived from the same material. Although all cobbles appear blue in the L256 color composite, the R267 decorrelation stretch shows at least two types of cobbles: red and purple. The purple cobbles have a slightly steeper downward slope between 673 and 904 nm and a stronger upturn between 934 and 1009 nm relative to Antistasi (Figure 23, Little Cobble). These purple cobbles have spectra very similar to the blueberries, although they appear larger and more irregular in shape than typical spherules that make up the blueberry population. They could represent Antistasi-like material with more hematite. The outcrop matches the HFS spectral unit identified by *Farrand et al.* [2007] for flat-lying outcrop exposures at Meridiani Planum.

3.8. Santa Catarina (Sols 1045–1055)

[37] Santa Catarina is a 14 cm long cobble found along the rim of Victoria crater. MI images (Figure 24) show jagged edges and large, bright rounded clasts that appear to be phenocrysts. Semicircular cavities and subplanar protrusions with highly irregular edges result in an angular surface. The cavities are consistent with abrasion through eolian activity or scouring by impact ejecta, while the irregularity of the protrusions is more consistent with these being a product of the underlying lithology. Qualitative

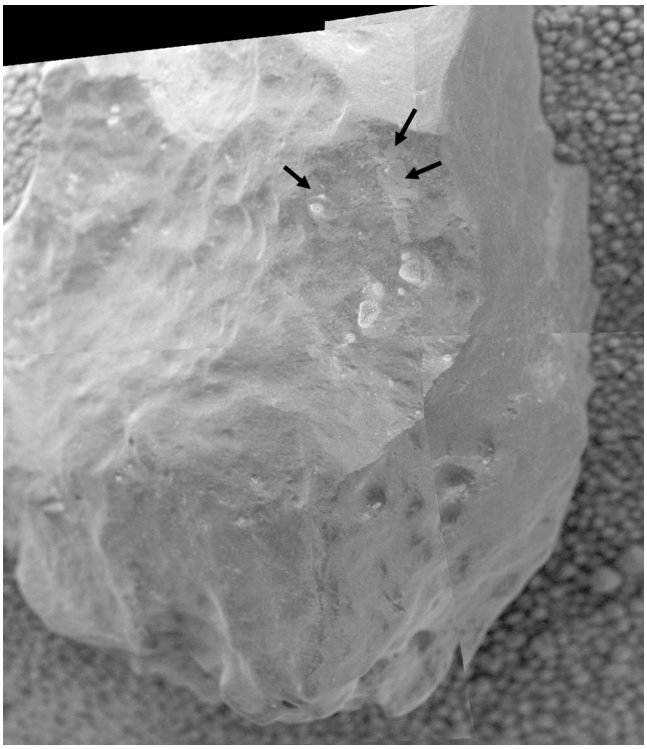

Figure 21. MI mosaic of the 10 cm cobble Antistasi. Black arrows identify rounded clasts in the darker matrix.

roundness of the cobble is angular to very angular. However, the sphericity of this cobble could not be determined based on MI images.

[38] APXS measurements indicate an ultramafic composition with high Ni contents. MB measurements show more olivine than pyroxene, similar to Barberton, as well as the mineral troilite [*Schröder et al.*, 2008; *Fleischer et al.*, 2010b]. The geochemistry is consistent with a stony meteorite.

[39] Unfortunately, the rover was so close to the rock that the left side of the rock is only visible in the Pancam left filters while the right side of the rock is seen only in the right filters (Figure 24). Only the center of the rock has the full spectral range with all 13 bands. In the decorrelation stretch images, the upper surface of the rock has considerable eolian debris. The blueberries and outcrop have spectra (Figure 25) consistent with these same units found elsewhere at the landing site.

[40] The clasts in the rock that appear to be phenocrysts are spectrally distinct from the rock matrix. One phenocryst that has the full spectrum is shown in Figure 25. It has a steeper visible slope and a stronger long wavelength absorption than the rock matrix. Its spectrum is similar to the basaltic meteorite Bounce Rock, which indicates the phenocryst is likely a pyroxene based on the ~930 nm apparent absorption band center. The spectrum of the Santa Catarina matrix combined with pyroxene phenocrysts is consistent with a stony meteorite as measured by the geochemistry instruments.

3.9. Santorini (Sols 1741–1748)

[41] The 8 cm long cobble Santorini is located on outcrops to the south of Victoria crater (Figure 2). The cobble has a massive lithology, with angles and facets at both the centimeter scale and in MI images. Portions of its surface appear lustrous in MI images (Figure 26), although many fine particles probably represent dust and other eolian debris. The surface texture is dominated by somewhat blocky facets and angles. Some of these show a higher reflectance in Pancam images. The texture is similar to coarser-grained (millimeter scale), blocky, unweathered basalt clasts. Numerous pits are also visible, typically 300–400 μm in diameter. These pits have very angular edges, indicating they are not due to in situ wear, but are intrinsic to the lithology of the cobble itself. The sphericity is approximately 0.75, and the quantitative roundness is less than 0.15 (very angular clast). This indicates the cobble has not undergone significant wear during or after transport to its current location.

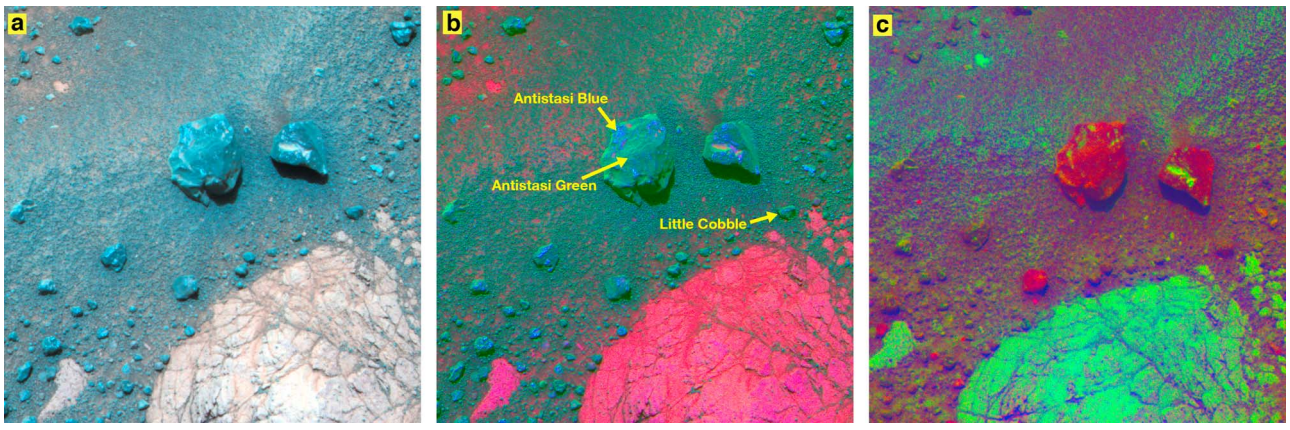

Figure 22. Pancam scene of Antistasi (largest) and several smaller cobbles. (a) L256 color of Antistasi and other blue cobbles. Outcrop exposures are also within the scene. (b) L257 decorrelation stretch image shows the cobbles have both blue and green colors. (c) R267 decorellation stretch image. Antistasi and several other cobbles appear red with small patches of green. Other cobbles appear dark purple like the blueberries that cover most of the soils here.

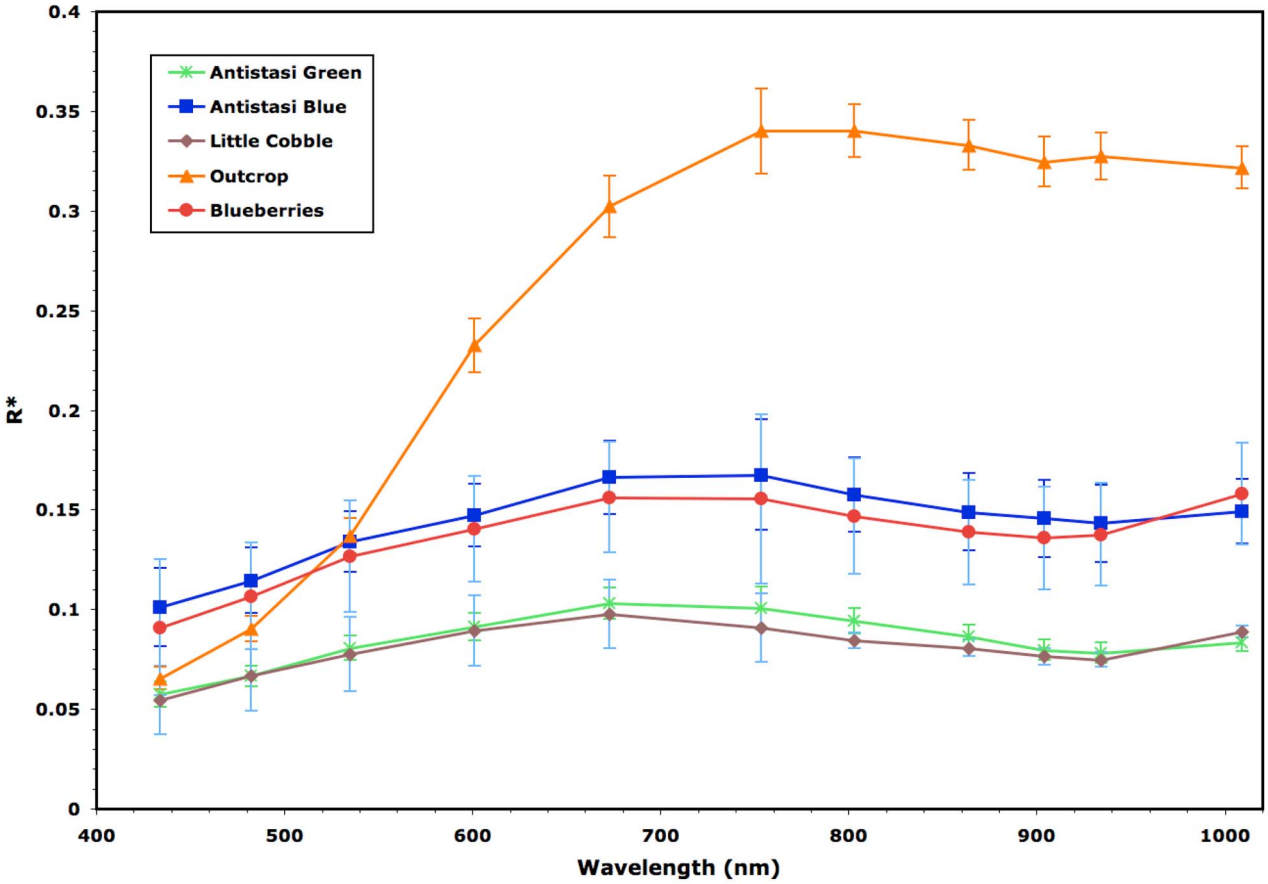

Figure 23. Pancam spectra of Antistasi and nearby rocks. A smaller cobble that appears purple in the R267 decorellation stretch image (Little Cobble) has a spectrum similar to the blueberries, indicating perhaps more hematite in some of the cobbles relative to the Antistasi type.

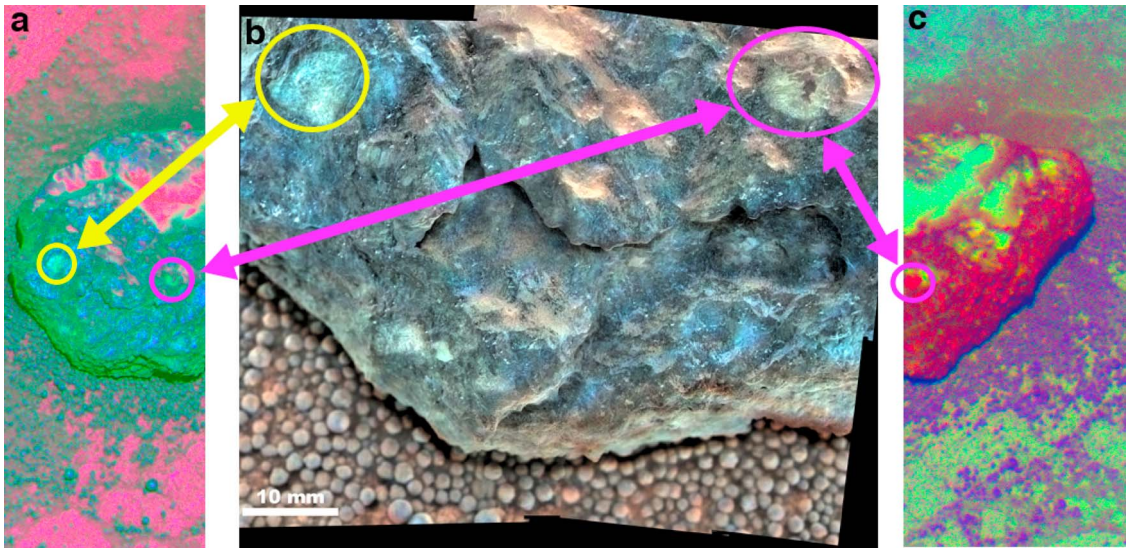

Figure 24. (a) L257 decorrelation stretch image of the left side of Santa Catarina with large phenocrysts circled. (b) MI mosaic merged with Pancam L257 color. The two large phenocrysts resolved in Pancam are circled. Only the phenocryst on the right side (purple circle) is visible in both the left and right Pancam filters. (c) R267 decorrelation stretch image of the right side of the cobble.

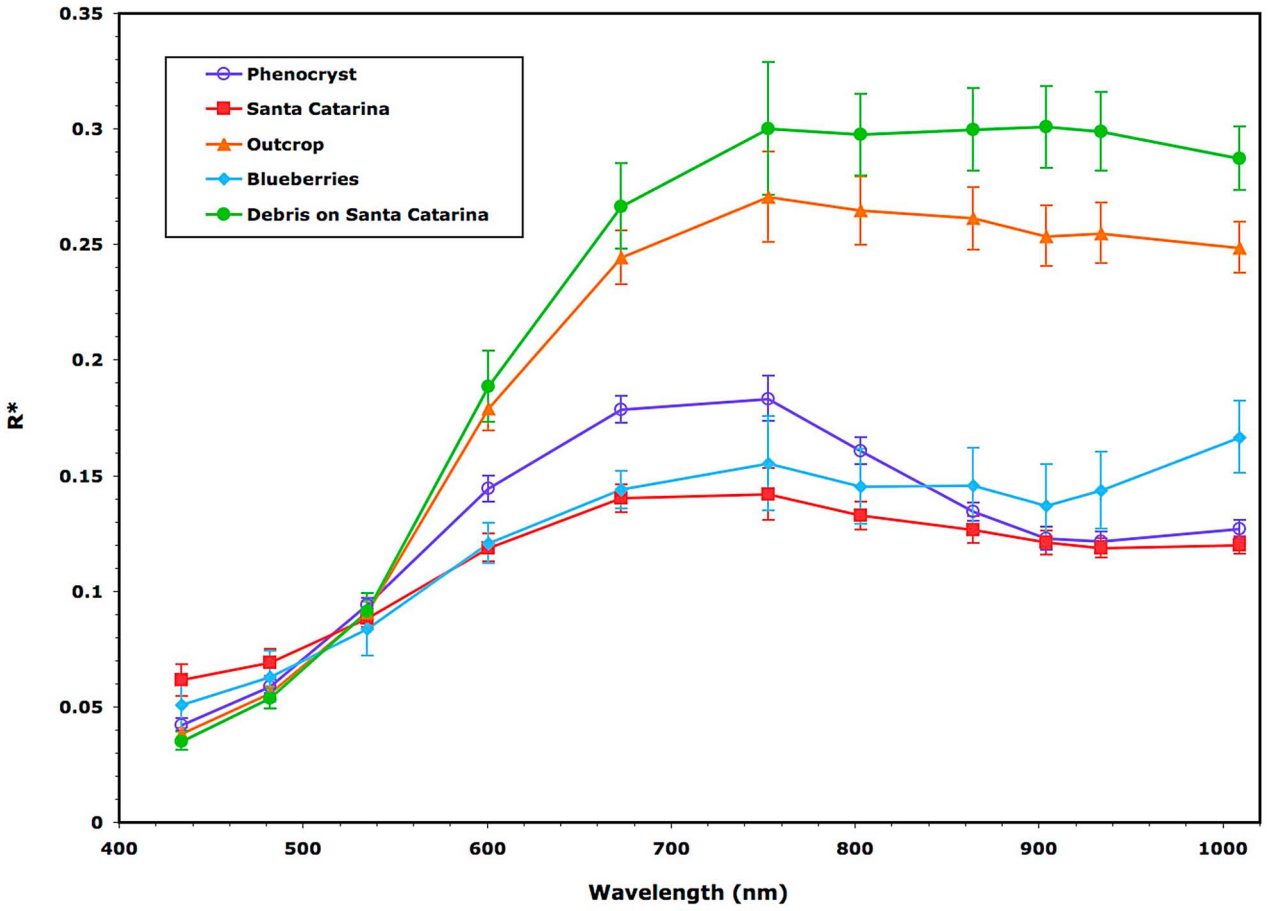

Figure 25. Pancam spectra taken of Santa Catarina and nearby rocks. The eolian debris seen on some top surfaces could be dust or outcrop-derived material. A large phenocryst within the cobble is spectrally consistent with pyroxene.

[42] APXS measurements show an ultramafic composition with high Ni and Cr similar to Santa Catarina, suggesting it is a meteorite. MB detected troilite with possible kamacite, along with olivine and pyroxene [*Schröder et al.*, 2010; *Fleischer et al.*, 2010b]. Fe oxidation states from the MB data suggest weathering [*Schröder et al.*, 2010].

[43] Pancam false color and decorrelation images reveal some color variations (Figure 27). There are areas of blue and green in the L257 decorrelation stretch image while the R267 decorrelation stretch image shows regions of red and green. Spectra from the cobble are shown in Figure 28. Spectral differences between blue and green areas in the L257 decorrelation stretch image are subtle and could be indicative of greater dust contamination in the green areas. The stronger 535 nm band depth in Santorini 1 could indicate the presence of higher abundances of oxides as shown by the MB measurements.

[44] The outcrop is consistent with the flat-lying HFS type from *Farrand et al.* [2007], although there is an unusual absorption around 800 nm not typically seen in outcrop, perhaps an instrumental effect. The blueberries show the characteristic strong upturn between 934 to 1009 nm. Several of the centimeter size nearby cobbles are spectrally similar to Santorini but others differ. In particular, a cobble that appears bright red in the R267 decorrelation stretch (Figure 27, Little Cobble 2) has a strong absorption at the longer wavelengths, perhaps due to pyroxene. Little Cobble 1 does not have the downward slope between 934 to 1009 nm found in the Santorini spectra, suggesting a different mineralogy.

3.10. Kos, Tilos, and Rhodes (Sols 1877–1882)

[45] These three pebbles are clustered along with other smaller pebbles to the south of Victoria crater. Each pebble is a few cm across and has been measured by APXS only. Pebble surface textures are difficult to discern due to the very low contrast of MI images. However, they appear similar: smooth and relatively featureless (Figure 29). No individual grains are present. Kos has submillimeter-scale pits, with smoothed rims. Rhodes is about 4 cm in size with a sphericity of 0.79 and a roundness of 0.54 (rounded to well rounded). Tilos is 1.5 cm in size with a sphericity of 0.79 and a roundness of 0.61 (rounded). Kos is about 1 cm in size with a sphericity of 0.86 and a roundness of 0.81 (well rounded).

[46] Their composition is best matched to a mixture of dust and basaltic soil. None of the cobbles show enrichment of Ni. However, due to uncertainties in the placement of the APXS for Tilos and Kos, as well as the comparatively large

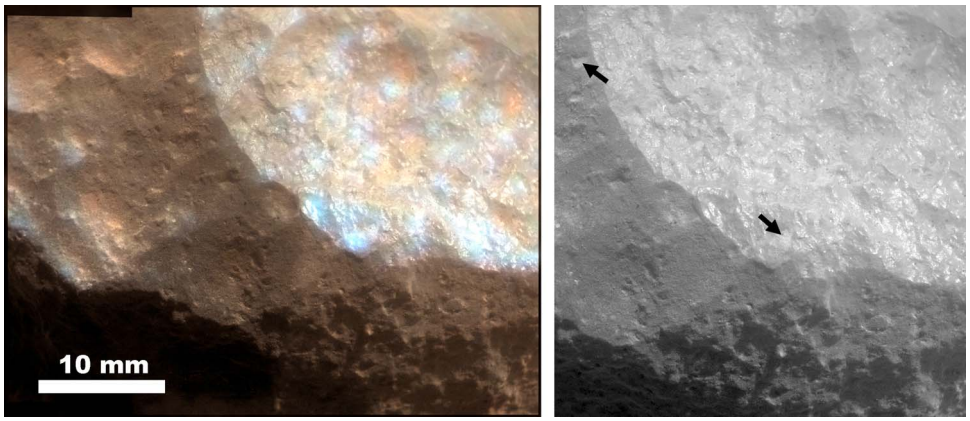

Figure 26. (left) Pancam L257 color merged with MI mosaic of Santorini and (right) portion of MI image where arrows point to possible phenocrysts.

4 cm offset in standoff distance from the pebbles (normal APXS standoff distances are 1–2 cm), adjacent soil (basaltic sand, blueberries, and dust) was measured along with the pebbles. Because no MB was acquired for any of these pebbles and because there is contamination in the APXS measurements by soil components, the precise mineralogy is unconstrained.

[47] All three pebbles appear blue in the L256 color composite and L257 decorrelation stretch images (Figure 30). They have similar spectra (Figure 31) and were most likely derived from the same parental material. Most of the smaller pebbles in the same Pancam scene appear spectrally similar to these three pebbles. The pebble mineralogy cannot be determined from their spectra due to the lack of diagnostic absorption features. The outcrops have spectra consistent with flat-lying HFS spectral class from *Farrand et al.* [2007]. The blueberries show a weaker absorption at the longer wavelengths compared to other spherules at the landing site, perhaps because their small size in this Pancam scene makes them difficult to resolve, or because of air fall dust.

3.11. Kasos (Sols 1884–1890)

[48] Kasos is only a few meters away from Kos, Tilos and Rhodes (Figure 2). It is about 8 cm across. In the MI images (Figure 32), the rock has a glassy, lustrous appearance. There appear to be both bright and dark surfaces on the rock but it is difficult to decipher if the bright areas are dust covered or represent brighter crystals within a darker matrix. Alternatively, darker and lighter areas could be products of differing response of topography to illumination. The cobble has a grainy texture, more fine scale than the blockier, more massive texture seen in Santorini and lacking the arcuate features and flaky texture of Santa Catarina. The sphericity is a rather high 0.86, indicating it to be nearly equant. Quantitative roundness is less than 0.13 (very angular).

[49] The composition is very similar to Santorini with high Mg and Ni. However, the Fe mineralogy is different from Santorini, Barberton, and Santa Catarina with more

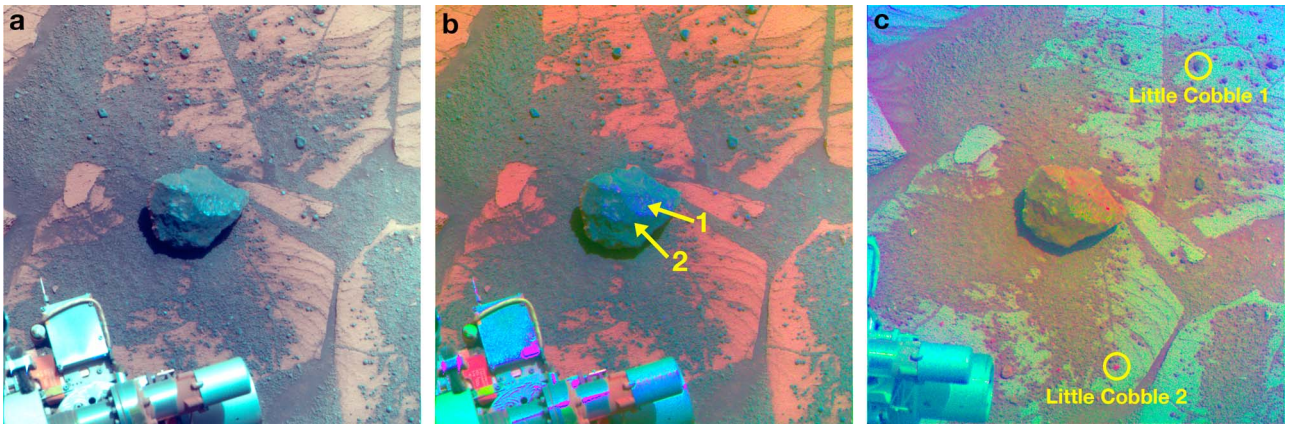

Figure 27. (a) L256 composite of Santorini cobble. Numerous smaller cobbles as well as blueberries are also visible in the scene. A portion of the rover arm and instruments obscures the bottom of the image. (b) L257 decorrelation stretch image shows blue and green colors for the cobble. Numbers identify locations where spectra were extracted. (c) The cobble appears red and green in this R267 decorrelation stretch image. Two smaller cobbles where spectra were extracted are identified.

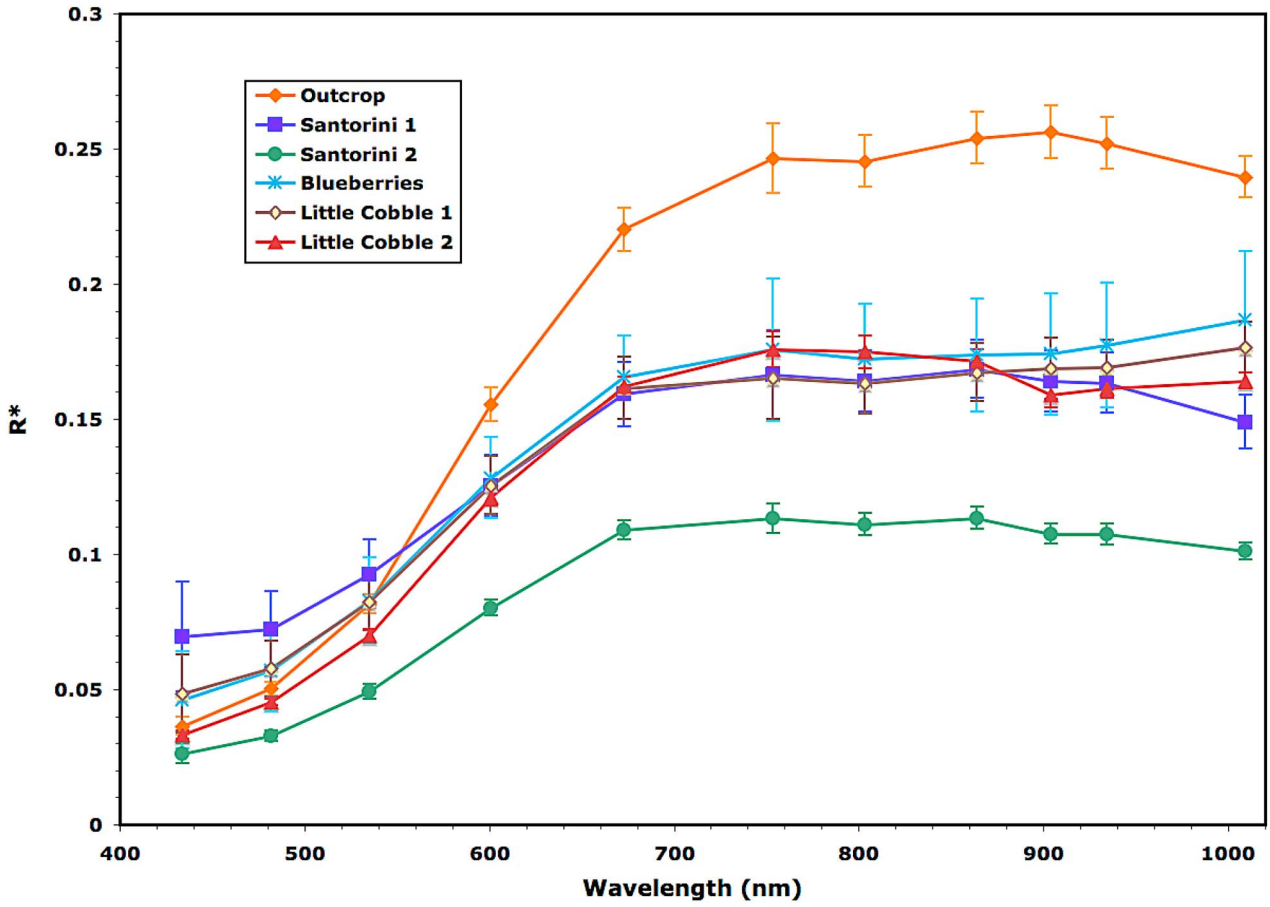

Figure 28. Two spectra extracted from Santorini correspond to the blue (Santorini 1) and green (Santorini 2) regions shown in the L257 decorrelation stretch (Figure 27b). Also shown are spectra from two smaller cobbles. Both smaller cobbles are spectrally distinct from Santorini.

pyroxene relative to olivine [*Fleischer et al.*, 2010b]. There is a troilite signature in the MB spectra, consistent with a meteorite origin. *Schröder et al.* [2010] propose that Barberton, Santa Catarina, Santorini, and Kasos are fragments of the same larger body given their similar chemistry. Because the fragments are separated over a 10 km distance, they could be part of a meteorite strewn field, or fragments spalled off from the impactor that created Victoria crater.

[50] Pancam color images do not show any heterogeneities in the rock except where there may be accumulations of dust (Figure 33). The spectrum of Kasos has a relatively strong 535 nm band depth and a downward slope from 673 nm to 1009 nm (Figure 34). Two other smaller cobbles appear spectrally distinct which suggests there may be multiple rock compositions at this location. Cobble 1 appears purple while cobble 2 appears bright red in the R267 decorrelation stretch (Figure 33). Cobble 1 is spectrally distinct from Kasos while cobble 2 could contain pyroxene. The blueberries lack a broad absorption at the longer wavelengths and a pronounced upturn between the 934 and 1009 nm wavelengths that are characteristics of the blueberries elsewhere at the landing site. However, the small size of the blueberries in this Pancam scene may limit our ability to adequately sample their spectra or they could be coated with dust.

3.12. Block Island (Sols 1961–2003)

[51] Block Island is a 60 cm diameter pitted boulder discovered along the plains toward Endeavor crater. The geochemistry indicates a FeNi meteorite with enrichment in S, Cl, and P. Block Island may have originated from the same parental meteorite as Heat Shield Rock based upon their identical compositions [*Fleischer et al.*, 2010a]. False color decorrelation stretch images reveal spectral heterogeneities across the surface (Figure 35), although much of the surface is dust covered. The surface texture is metallic, with numerous hallows and caverns giving it a pitted appearance. Much of the surface, especially within the caverns, is mantled with a thin coating of dust, while the larger caverns also contain sand and blueberries. The largest cavern is 20 cm across and is rimmed by metal protuberances that could have formed by acidic corrosion (J. W. Ashley et al., submitted manuscript, 2010). MI images are consistent with the metallic, meteoritic nature of the rock, showing slightly raised (resistant) linear features indicative of the Widmanstätten pattern common to iron-nickel meteorites (Figure 36). Qualitative roundness of the meteorite is very angular while

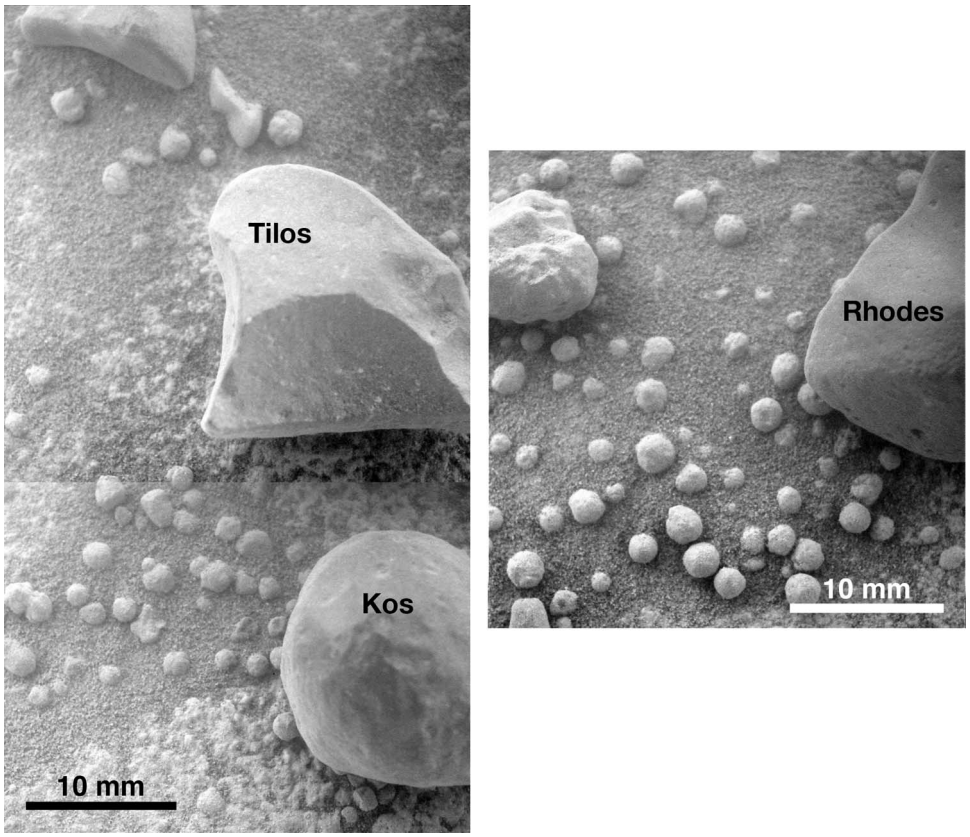

Figure 29. MI images of the cobbles Tilos, Kos, and Rhodes. Kos is spherical while the other cobbles are angular. Other smaller cobbles as well as the blueberries are also visible.

sphericity is a very low 0.6, comparable to freshly broken grains.

[52] In general, spectra of Block Island are bland and similar to soil and sand (Figure 37). Relative to the green areas, the purple regions appear lobate and are unlikely to be fushion crusts (J. W. Ashley et al., submitted manuscript, 2010) more probably representing weathering rinds instead [*Ashley et al.*, 2010; *Johnson et al.*, 2010]. The purple areas have a greater 535 nm band depth but flatter NIR slopes relative to the green regions, suggesting more oxidation [*Johnson et al.*, 2010] and consistent with MB data that indicate phases of ferric oxide that have undergone a low

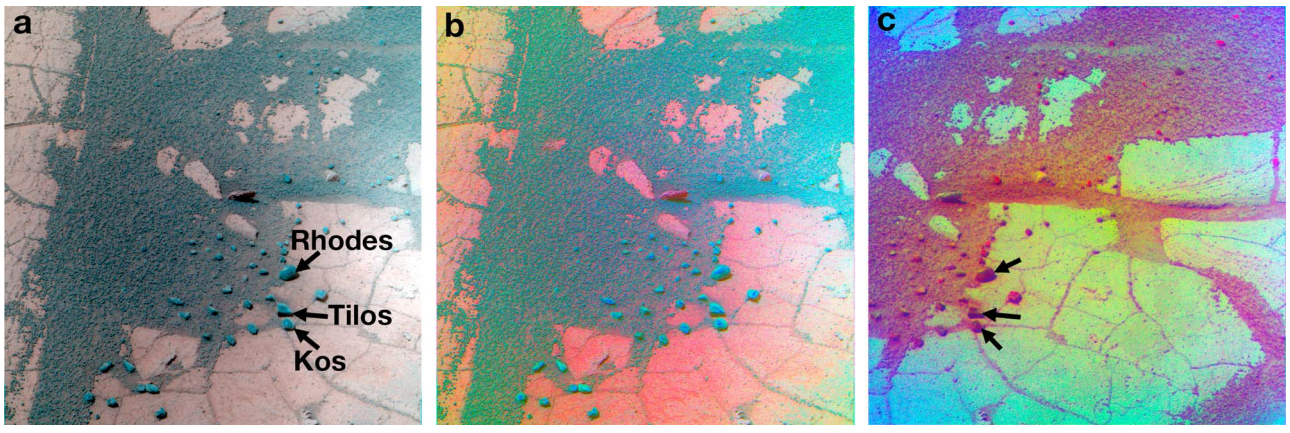

Figure 30. Pancam scene of the cobbles Rhodes, Tilos, and Kos. (a) L256 composite image with the locations of the three cobbles. Numerous other cobbles are also visible in the image. (b) L257 decorrelation stretch image. (c) R267 decorrelation stretch image. All the cobbles appear similar in color and could have been derived from the same parental material.

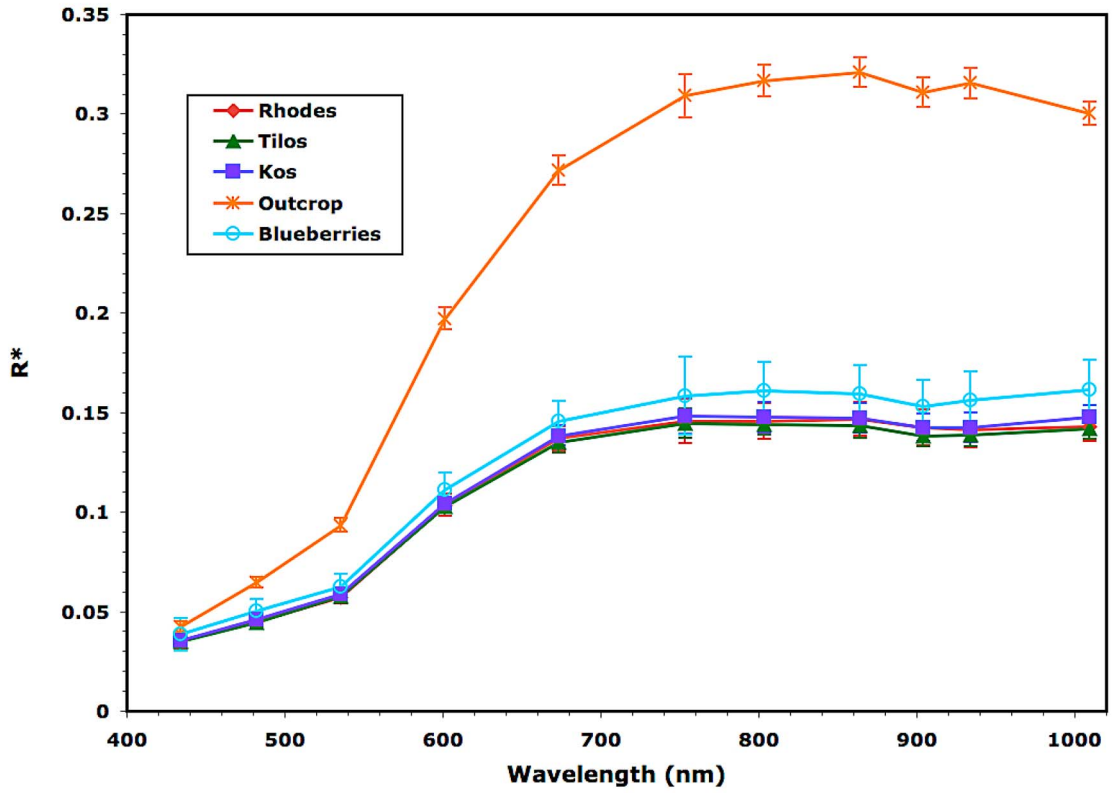

Figure 31. Spectra of Rhodes, Tilos, and Kos are similar, suggesting they represent the same rock type.

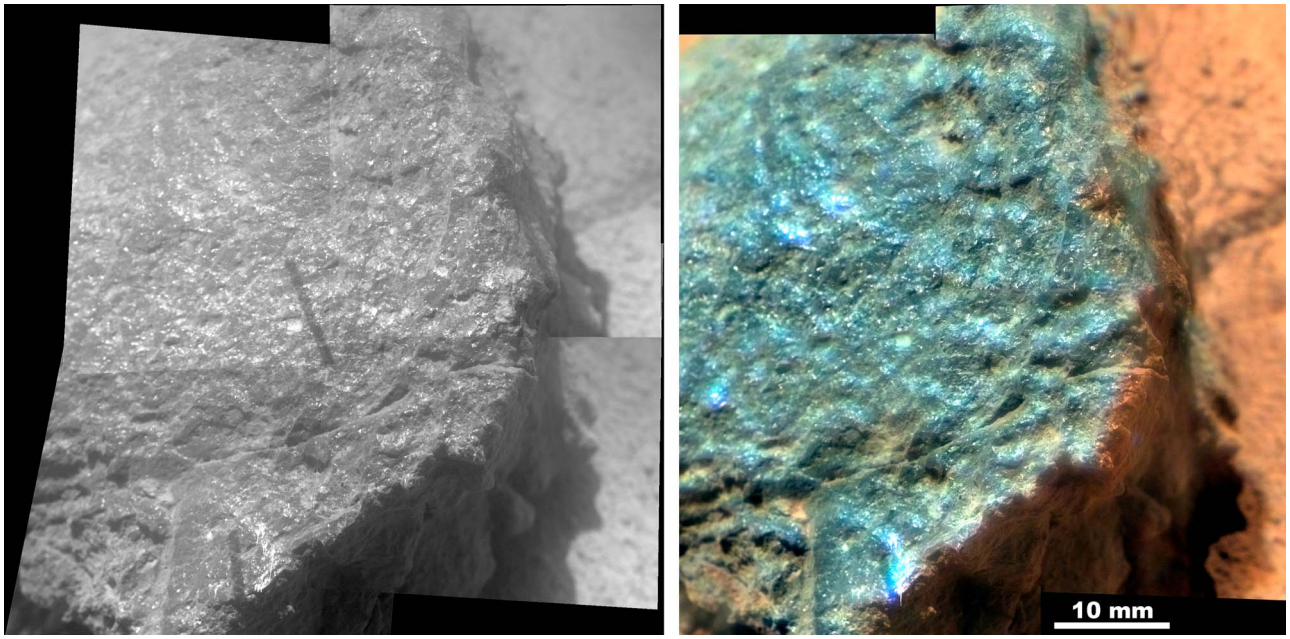

Figure 32. Mosaic of MI images (left) for the cobble Kasos and (right) merged with Pancam L257 color. The cobble has a glassy, lustrous appearance.

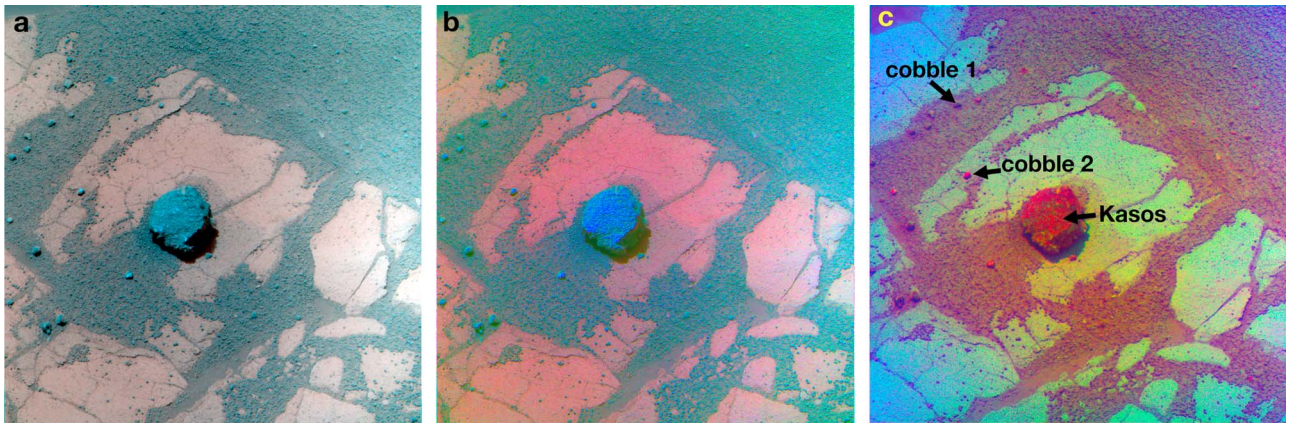

Figure 33. (a) L256 composite shows Kasos resting on outcrop exposure. (b) L257 decorrelation stretch does not reveal any heterogeneities across Kasos. (c) R267 decorrelation stretch of Kasos and two smaller cobbles.

degree of chemical weathering [*Fleischer et al.*, 2010a]. Similar coatings of ferric oxides were also seen in spectra of Heat Shield Rock [*Schröder et al.*, 2008]. Note that the blueberries spectrum has a downturn between 934 to 1009 nm, unlike the typical upturn seen in blueberries elsewhere at the landing site. A dust coating on the surfaces of the blueberries could explain their unusual spectra at this location.

4. Discussion

[53] In order to quantify color differences between the rock fragments, we have applied a set of spectral parameters

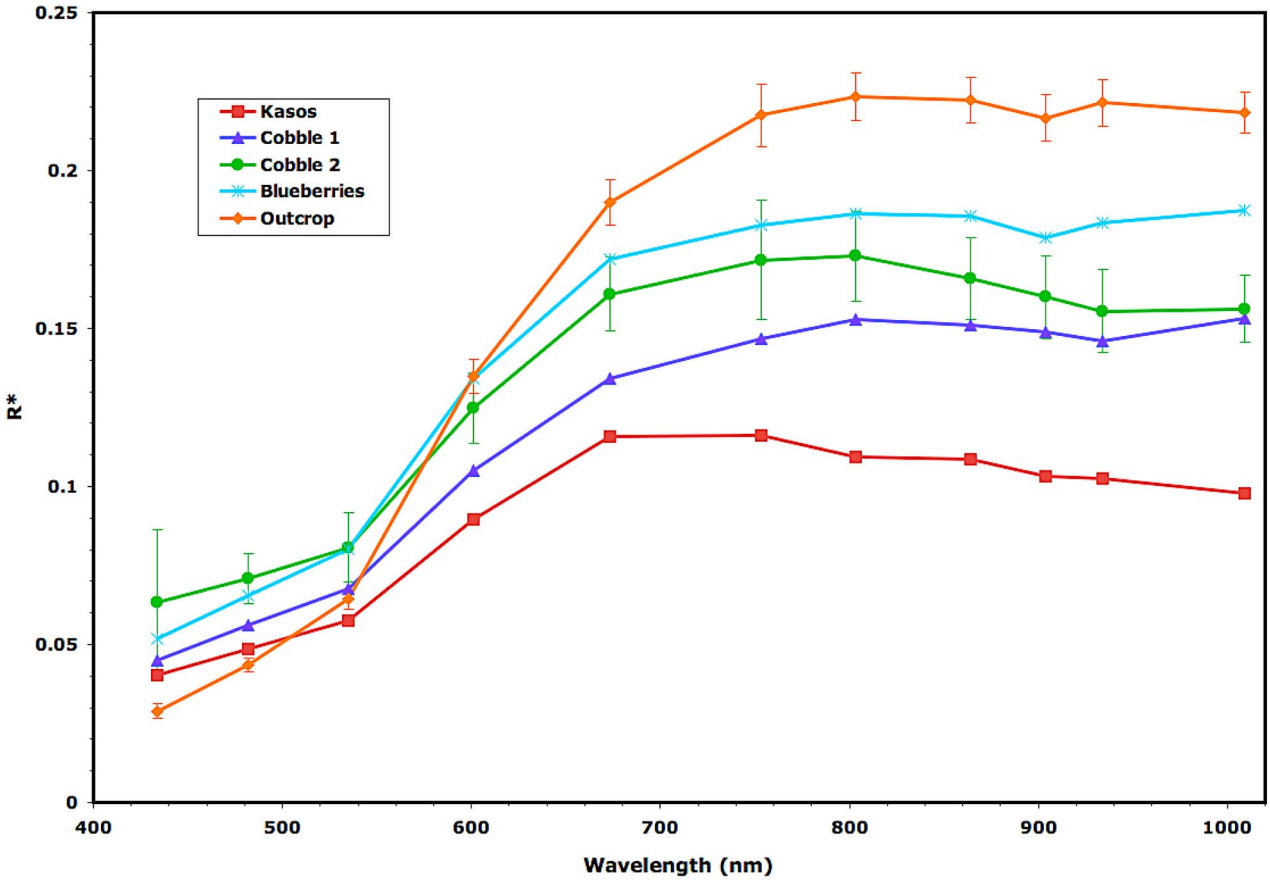

Figure 34. Spectra of Kasos and other nearby cobbles.

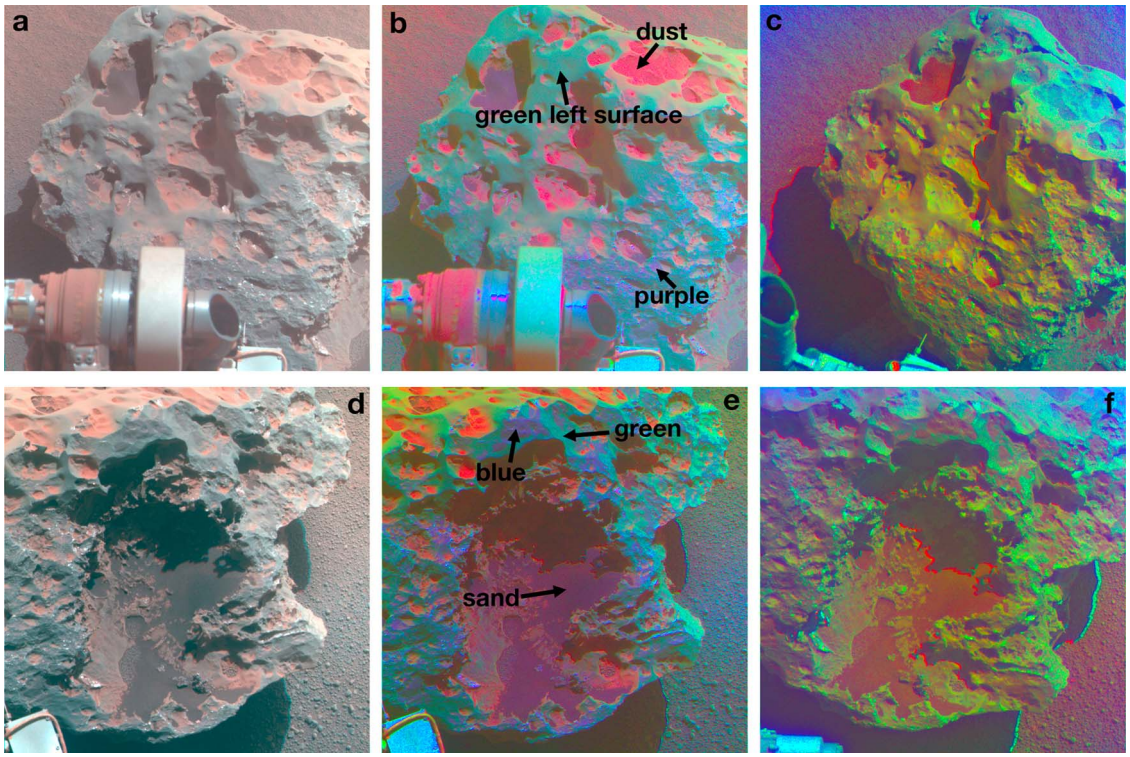

Figure 35. Left and right side views of the boulder Block Island. (a) L256 composite of the left side with a portion of the robotic arm in the lower left. (b) L257 decorrelation stretch image with locations of some surfaces where spectra were extracted and shown in Figure 37. (c) R267 decorrelation stretch image. (d) L256 color composite of the right side of Block Island and a small portion of the rover deck in the lower left. A large cavern is partially filled with sand and dust. (e) L257 decorrelation stretch with locations of some surfaces where spectra were extracted and shown in Figure 37. (f) R267 decorrelation stretch image.

selected on the basis of their ability to highlight unique spectral differences between the rocks. Table 2 lists the spectral parameters for this study. Materials with high 535 nm band depth values are generally outcrop or dusty. The inflection in the spectral slope at the 535 nm band can be used to measure the degree of crystallinity of ferric oxide minerals and/or particle size. The 535 nm band depth parameter has also been found to have a direct relation to the Fe^{3+}/Fe_{Total} value returned by in situ measurements of rocks by the Spirit rover's Mössbauer spectrometer [*Farrand et al.*, 2006, 2008]. The red/blue (753/432 nm) ratio and 482 to 673 nm slope are important discriminators of the degree of oxidation. The 934/1009 nm ratio is useful for identifying the inflection at the longest wavelengths. Hematite-rich blueberries are best seen by low 934/1009 nm values. The 754–864 nm slope and the 754–1009 nm slope are used to determine the strength and position of the NIR absorption. The 803/904 nm ratio is also used to determine the strength of the NIR absorption. Spectral parameter plots for all rock fragments are shown in Figure 38.

[54] We have also calculated spectral parameters for blueberries and outcrop from the same Pancam scenes that contain rock fragments. In addition, a typical soil with no blueberries along the Meridiani plains (sol 68 soil) and some darkish sand trapped within a Block Island pit (sand in Block Island) are plotted for comparison. Finally, we show the pre-RAT and RAT'ed blueberries at two locations in order to infer possible chemical alteration or dust cover. After the RAT ground away a portion of a few blueberries in the outcrop, we assume that the spectra extracted from the cut blueberries represents clean material (i.e., no dust or atmospheric alteration). The plots do show that the RAT'ed blueberries have higher 754 to 1009 nm slopes and an increase in the 535 nm band depth relative to the non-RAT'ed blueberries, consistent with hematite-rich materials. We note that the RAT'ed blueberries from each site (sols 35 and 405) do not always plot close together even though they are likely the same in composition. These observations suggest that other factors, such as illumination geometry and/or residual dust, affect spectra and calculated spectral parameters.

[55] The iron meteorites (Table 3), Heat Shield Rock and Block Island, have spectral heterogeneities due to patches of ferric oxide coatings as well as eolian debris on their surfaces. The purple RAT brushed region on Heat Shield Rock (Figure 38, Heat Shield Brushed 2) and the unbrushed purple region on Block Island have greater 535 nm band depths relative to other areas on the meteorites, consistent with some type of ferric oxide. The blue and purple patches on each rock have slightly higher 904 nm band depths and 803/904 nm ratios than the typical greener surfaces on the meteorites. Relative to other rock fragments, the iron meteorites have generally lower 904 nm band depths and 803/904 nm ratios and higher 754 to 864 nm slopes.

[56] The four stony meteorites with similar geochemistry (Table 3; Barberton, Santorini, Santa Catarina, and Kasos)

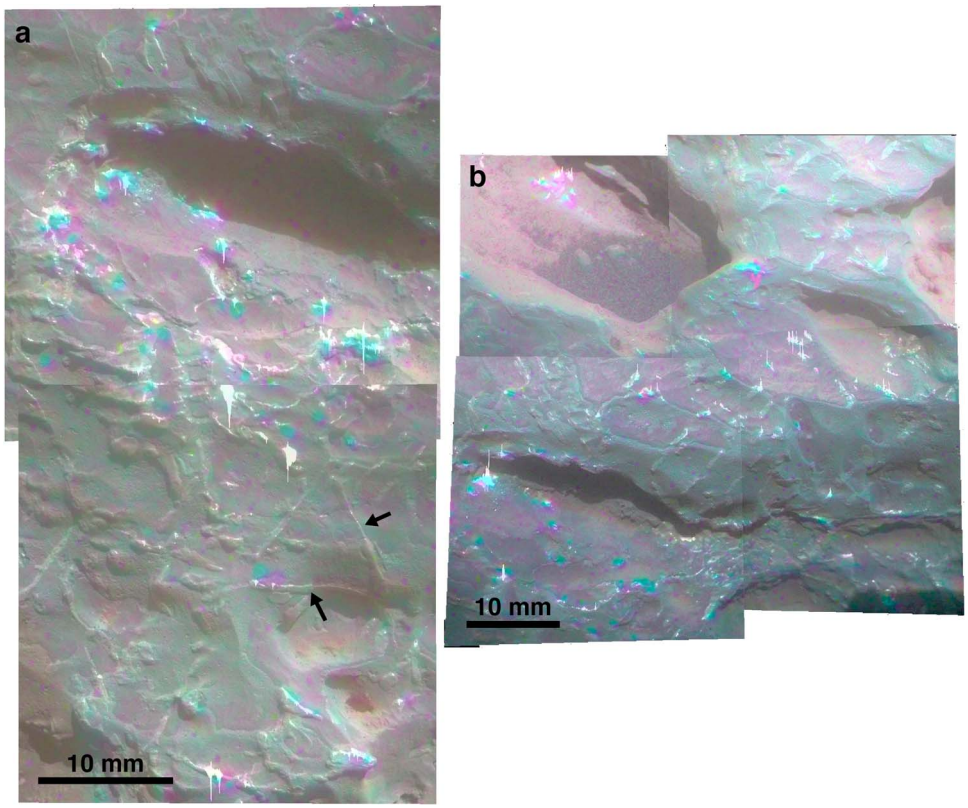

Figure 36. MI mosaics acquired along the left side of Block Island. The L257 decorrelation stretch image has been overlain to show color. Arrows identify raised linear features characteristic of Widmanstätten pattern. The purple areas correspond to lobate smooth regions within the green matrix.

have distinct spectral parameters. Two spectra extracted from Barberton have different 934/1009 nm ratios and 482 to 673 nm slopes, suggesting mineralogic heterogeneities within individual rock fragments. As noted previously, the two spectra differ significantly in the longest wavelengths with Barberton 1 showing a downturn between 934 to 1009 nm whereas Barberton 2 has an upturn. The other stony meteorites plot closer to Barberton 1 with a high 934/1009 nm ratio, suggesting that Barberton 2 may be anomalous. Because the 535 nm band depth is similar for both Barberton locations and slightly lower than the other stony meteorites, dust contamination may not be the cause of the spectral variations on Barberton. Relative to all the other rock fragments, the stony meteorites lie in the middle for all spectral parameters.

[57] Bounce Rock, an impact ejecta fragment dominated by basalt, has the lowest 754 to 1009 nm and 754 to 864 nm slopes and highest 803/904 nm ratio relative to all other units at the Meridiani Planum landing site. Pancam spectra support a basaltic composition and the spectral parameters differentiate Bounce Rock from all other rock fragments seen at the landing site thus far (through sol 2004). The rock fragments Lion Stone and Russett have spectral properties characteristic of outcrop exposures, although they have higher 904 nm band depths but lower 482 to 673 nm and 754 70 864 nm slopes and lower 934/1009 nm ratios compared to outcrop exposures. These differences could result from thinner weathering rinds on the two rocks relative to the outcrops. This hypothesis is consistent with work by *Farrand et al.* [2008] that distinguishes flatter buff-colored oxidized outcrops with weathering rinds (HFS spectral class) from steeper purple-colored less oxidized outcrops (LFS spectral class).

[58] Arkansas, Perseverance, Antistasi, Tilos, Kos, and Rhodes are also believed to be impact ejecta fragments with unknown origins (Table 3). Arkansas and Perseverance are spectrally similar with minor differences in the 904 nm band depth and 934/1009 nm ratio. Kos, Tilos, and Rhodes cluster together in all four spectral parameter plots. Relative to Arkansas and Perseverance, they have higher 535 nm band depths, 482 to 673 nm slopes, and 753/432 ratios. These higher values could reflect thicker dust coatings because the values plotted for Arkansas and Perseverance are from the sides of the rocks whereas the spectra extracted from the smaller Kos, Tilos, and Rhodes pebbles covers both upper and side surfaces. Antistasi appears to have the most unique spectral parameters relative to these five other impact fragments. It has spectral parameter values close to Bounce Rock, including a low 535 nm band depth, high 904 nm band depth, high 803/904 nm ratio, and low 754 to 1009 nm slope. One possibility is that the spectra were extracted in a region that had pyroxene and/or olivine crystals, consistent with a larger basaltic contribution measured by MB [*Fleischer et al.*, 2010b]. Based upon the spectral characteristics, Antistasi mineralogy appears to be distinct from the other impact fragments, consistent with

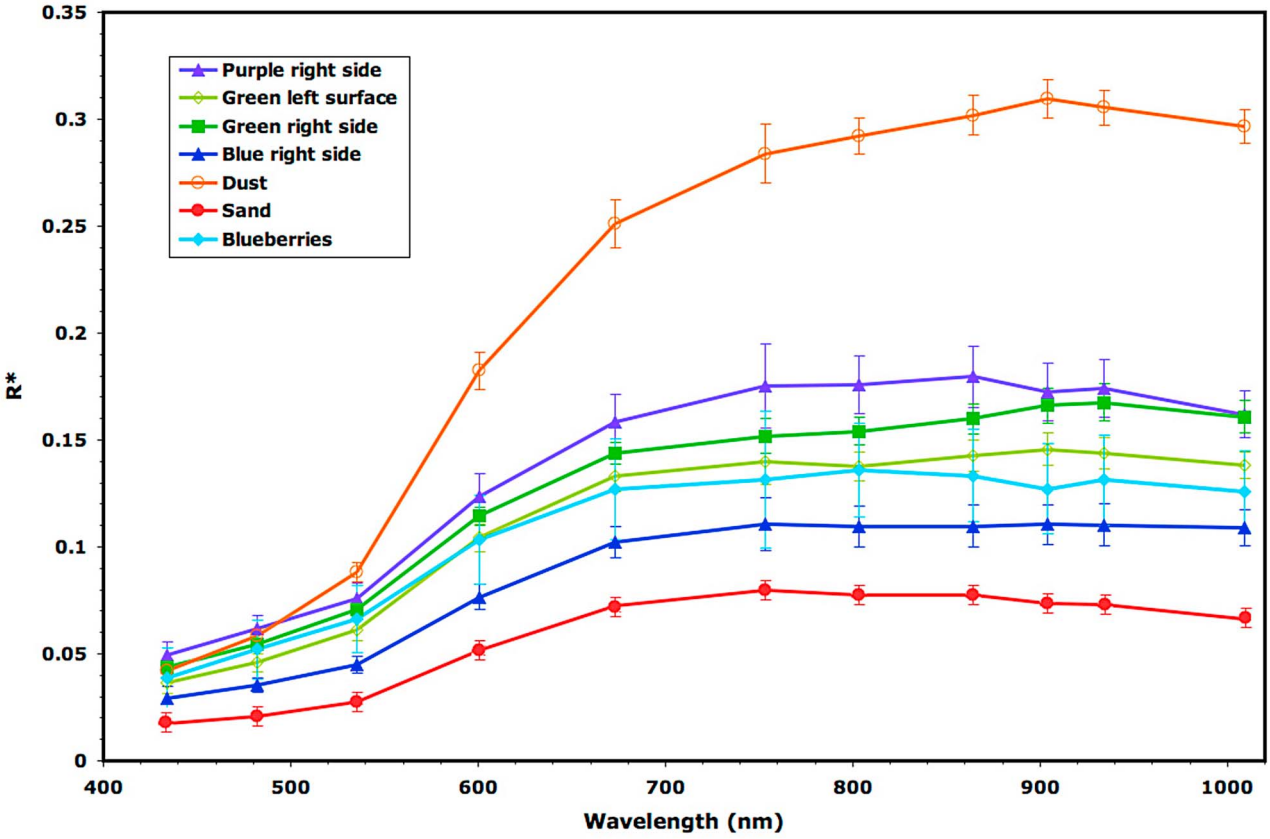

Figure 37. Block Island spectra. The purple areas have greater 535 nm band depths but flatter NIR slopes relative to the green regions.

APXS data that distinguish the rock from other Arkansas group cobbles [*Fleischer et al.*, 2010b].

5. Conclusions

[59] Our results suggest that examination of rock fragments using multispectral reflectance data can prove useful for an initial assessment of rock classification and provide guidance on whether a rock should receive additional measurements due to spectral and/or physical properties that are deemed of high scientific interest. Generally, rock fragments that appear dark toned and bluish in Pancam left eye false color color composites are differentiated from outcrop rocks and likely to be considered for further investigation. Physical properties of these rock fragments, including sphericity, roundness, and evidence for pits, can also be explored with Pancam images. However, in situ examination to determine mineralogy and small-scale textural information is critical for a definitive composition and origin.

[60] The results from our investigation of 15 rock fragments at the Opportunity landing site reveal that the complexities of viewing and lighting geometry, combined with dust coatings, possible weathering rinds, residual fushion crusts in the case of meteoritic fragments, and sampling size, all affect the ability to adequately characterize the mineralogy of the rocks using Pancam's eleven visible/near-infrared bands. Most of the rock fragments have no diagnostic visible/near-infrared signatures in the Pancam data that would allow us to confidently determine the mineralogy. Bounce Rock is an exception because its spectrum has a pyroxene absorption that supports a basaltic composition unlike any other rock

Table 2. Description of Spectral Parameters Used in This Study

Parameter	Description	Characteristic
535 nm band depth	$1–[R_{535}/((0.57*R_{434})+(0.43*R_{673}))]$	Degree of oxidation
482 to 673 nm slope	$(R_{673}–R_{482})/(673–482)$	Degree of oxidation
904 nm band depth	$1–[R_{904}/((0.51*R_{803})+(0.49*R_{1009}))]$	Strength of NIR absorption
803/904 nm ratio	R_{803}/R_{904}	Strength of NIR absorption
754 to 864 nm slope	$(R_{754}–R_{864})/(864–754)$	Strength and position of NIR absorption
754 to 1009 nm slope	$(R_{754}–R_{1009})/(1009–754)$	Strength and position of NIR absorption
753/432 nm ratio	R_{753}/R_{432}	Red to blue ratio
934/1009 nm ratio	R_{934}/R_{1009}	Hematite

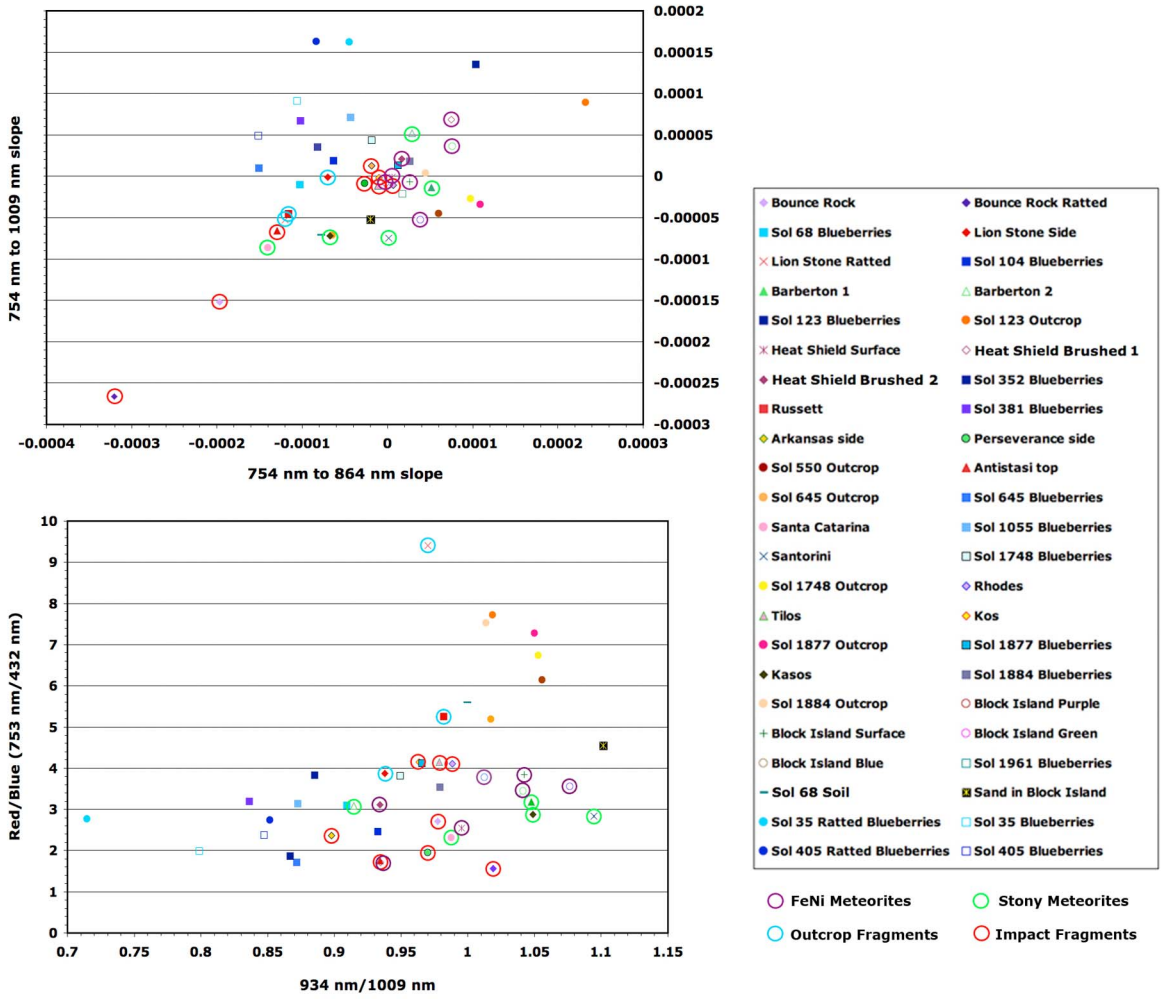

Figure 38. Spectral parameter plots for rock fragments and other geologic units at Meridiani Planum (see text for a discussion).

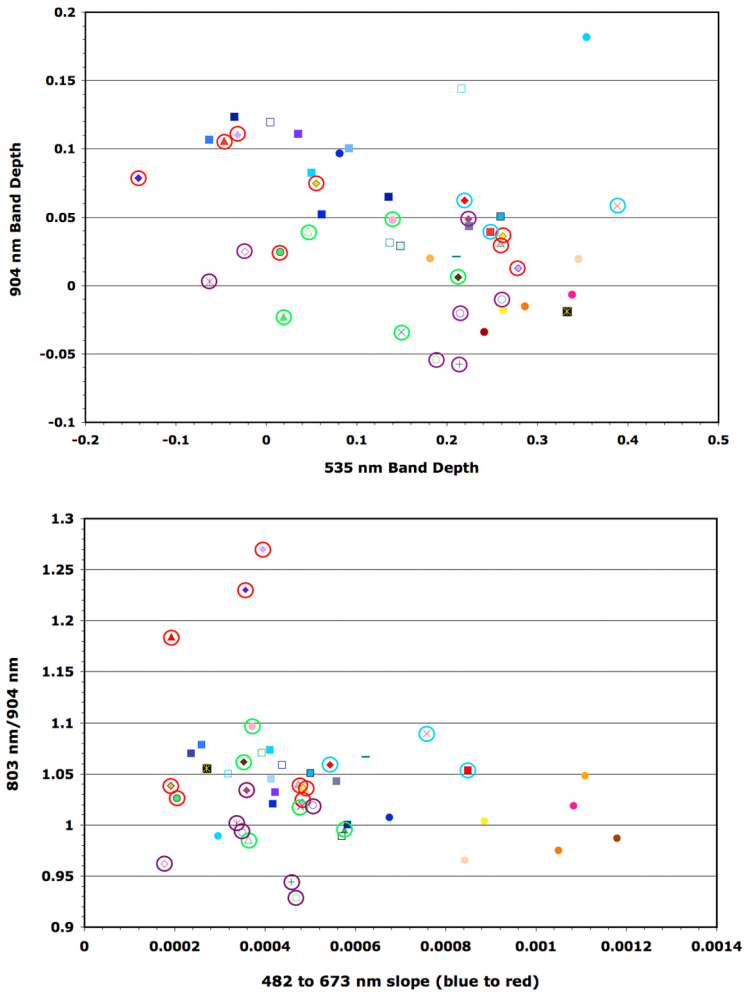

Figure 38. (continued)

seen at Meridiani Planum thus far. The stony meteorites and other impact ejecta fragments are too spectrally ambiguous to allow a specific mineralogic classification. However, rock fragments from the same Pancam scene can be differentiated, suggesting that spectral data is useful for distinguishing differences in rocks in any given spot at the landing site. For example, in decorrelation stretches that contain dozens of small pebbles, color differences are visible and extracted

Table 3. Summary of Rock Fragments

Name	Major Mineralogy Derived From MB	Rock Group and Proposed Origin
Bounce Rock	Olivine, Pyroxene	Basaltic shergottite
Lion Stone	Olivine, Pyroxene, Ferric Oxide, Jarosite, Hematite	Outcrop fragment
Russet	Olivine, Pyroxene, Ferric Oxide, Jarosite, Hematite	Outcrop fragment
Barberton	Olivine, Pyroxene, Nanophase ferric oxide, Kamacite, Troilite	Barberton Group, Stony meteorite
Santa Catarina	Olivine, Pyroxene, Nanophase ferric oxide, Kamacite, Troilite	Barberton Group, Stony meteorite
Santorini	Olivine, Pyroxene, Nanophase ferric oxide, Kamacite, Troilite	Barberton Group, Stony meteorite
Kasos	Olivine, Pyroxene, Nanophase ferric oxide, Kamacite, Troilite	Barberton Group, Stony meteorite
Arkansas	Olivine, Pyroxene, Nanophase ferric oxide, Ilmenite, Hematite	Arkansas Group, Impact ejecta
Perseverance	(no MB)	Arkansas Group, Impact ejecta
Antistasi	Olivine, Pyroxene, Nanophase ferric oxide, Ilmenite	Arkansas Group, Impact ejecta
Kos	(no MB)	Arkansas Group, Impact ejecta
Tilos	(no MB)	Arkansas Group, Impact ejecta
Rhodes	(no MB)	Arkansas Group, Impact ejecta
Heat Shield Rock	Kamacite, Ferric Oxide	Fe-Ni meteorite
Block Island	Kamacite, Ferric Oxide	Fe-Ni meteorite

spectra suggest that minor compositional variations may exist, such as more hematite in some pebbles. Unfortunately, the pebbles were too small for in situ measurements but they do indicate that numerous other rock assemblages may exist at the landing site but have not yet been geochemically analyzed. Hopefully, Opportunity will continue to make additional measurements on rock fragments at the site in order to further our understanding of the geologic processes that have operated and continue to occur in this region.

[61] **Acknowledgments.** We thank Onur Karahayit and Ron Li for producing the Opportunity traverse map and Ella Mae for providing several of the MI-Pancam color merges. Steve Ruff, Larry Soderblom, and an anonymous reviewer provided comments that improved the quality of this paper. We acknowledge the outstanding efforts of everyone on the JPL engineering and MER Athena science teams. This work was supported through NASA MDAP grant NNG05GB16G.

References

Ashley, J. W., M. P. Golombek, C. Schröder, I. Fleischer, T. J. McCoy, P. R. Christensen, and T. J. Parker, and the Athena Science Team (2010), Morphologic evidence for mechanical and chemical weathering of three new Iron-Nickel meteorites on Mars: Process insights for Meridiani Planum, *Lunar Planet. Sci.*, *XLI*, Abstract 2208.

Bell, J. F., III, et al. (2003), Mars Exploration Rover Athena Panoramic Camera (Pancam) investigation, *J. Geophys. Res.*, *108*(E12), 8063, doi:10.1029/2003JE002070.

Bell, J. F., III, et al. (2004), Pancam multispectral imaging results from the Opportunity Rover at Meridiani Planum, *Science*, *306*, 1703–1709, doi:10.1126/science.1105245.

Bell, J. F., III, J. Joseph, J. N. Sohl-Dickstein, H. M. Arneson, M. J. Johnson, M. T. Lemmon, and D. Savransky (2006), In-flight calibration and performance of the Mars Exploration Rover Panoramic Camera (Pancam) instruments, *J. Geophys. Res.*, *111*, E02S03, doi:10.1029/2005JE002444.

Christensen, P. R., et al. (2004), Mineralogy at Meridiani Planum from the Mini-TES experiment on the Opportunity Rover, *Science*, *306*(5702), 1733–1739, doi:10.1126/science.1104909.

Clark, B. C., et al. (2005), Chemistry and mineralogy of outcrops at Meridiani Planum, *Earth Planet. Sci. Lett.*, *240*, 73–94, doi:10.1016/j.epsl.2005.09.040.

Farrand, W. H., J. F. Bell III, J. R. Johnson, S. W. Squyres, J. Soderblom, and D. W. Ming (2006), Spectral variability among rocks in visible and near infrared multispectral Pancam data collected at Gusev Crater: Examinations using spectral mixture analysis and related techniques, *J. Geophys. Res.*, *111*, E02S15, doi:10.1029/2005JE002495.

Farrand, W. H., et al. (2007), Visible and near-infrared multispectral analysis of rocks at Meridiani Planum, Mars by the Mars Exploration Rover Opportunity, *J. Geophys. Res.*, *112*, E06S02, doi:10.1029/2006JE002773.

Farrand, W. H., J. F. Bell III, J. R. Johnson, R. E. Arvidson, L. S. Crumpler, J. A. Hurowitz, and C. Schröder (2008), Rock spectral classes observed by the Spirit rover's Pancam on the Gusev crater plains and in the Columbia Hills, *J. Geophys. Res.*, *113*, E12S38, doi:10.1029/2008JE003237.

Fleischer, I., G. Klingelhöfer, C. Schröder, D. W. Mittlefehldt, R. V. Morris, M. Golombek, and J. W. Ashley (2010a), In situ investigation of iron meteorites at Meridiani Planum, Mars, *Lunar Planet. Sci.*, *XLI*, Abstract 1791.

Fleischer, I., et al. (2010b), Mineralogy and chemistry of cobbles at Meridiani Planum, Mars, *J. Geophys. Res.*, *115*, E00F05, doi:10.1029/2010JE003621.

Gillespie, A. R., A. B. Kahle, and R. E. Walker (1986), Color enhancement of highly correlated images: 1. Decorrelation and HIS contrast stretches, *Remote Sens. Environ.*, *20*, 209–235, doi:10.1016/0034-4257(86)90044-1.

Gorevan, S. P., et al. (2003), Rock Abrasion Tool: Mars Exploration Rover mission, *J. Geophys. Res.*, *108*(E12), 8068, doi:10.1029/2003JE002061.

Grotzinger, J. P., et al. (2005), Stratigraphy, sedimentology and depositional environment of the Burns formation, Meridiani Planum, Mars, *Earth Planet. Sci. Lett.*, *240*, 11–72, doi:10.1016/j.epsl.2005.09.039.

Herkenhoff, K. E., et al. (2003), Athena Microscopic Imager investigation, *J. Geophys. Res.*, *108*(E12), 8065, doi:10.1029/2003JE002076.

Herkenhoff, K. E., et al. (2008), Surface processes recorded by rocks and soils on Meridiani Planum, Mars: Microscopic Imager observations during Opportunity's first three extended missions, *J. Geophys. Res.*, *113*, E12S32, doi:10.1029/2008JE003100.

Johnson, J. R., et al. (2006), Spectrophotometric properties of materials observed by Pancam on the Mars Exploration Rovers: 1. Spirit, *J. Geophys. Res.*, *111*, E02S14, doi:10.1029/2005JE002494.

Johnson, J. R., K. E. Herkenhoff, J. F. Bell III, W. H. Farrand, J. Ashley, C. Weitz, and S. W. Squyres (2010), Pancam visible/near-infrared spectra of large Fe-Ni meteorites at Meridiani Planum, Mars, *Lunar Planet. Sci.*, *XLI*, Abstract 1974.

Jolliff, B. L., W. H. Farrand, J. R. Johnson, C. Schröder, C. M. Weitz, and the Athena Science Team (2006), Origin of rocks and cobbles on the Meridiani Plains as seen by Opportunity, *Lunar Planet. Sci.*, *XXXVII*, Abstract 2401.

Klingelhöfer, G., et al. (2003), Athena MIMOS II Mössbauer spectrometer investigation, *J. Geophys. Res.*, *108*(E12), 8067, doi:10.1029/2003JE002138.

Klingelhöfer, G., et al. (2004), Jarosite and hematite at Meridiani Planum from Opportunity's Mössbauer spectrometer, *Science*, *306*, 1740–1745, doi:10.1126/science.1104653.

Knauth, L. P., D. M. Burt, and K. H. Wohletz (2005), Impact origin of sediments at the *Opportunity* landing site on Mars, *Nature*, *438*, 1123–1128, doi:10.1038/nature04383.

McCollom, T. M., and B. M. Hynek (2005), A volcanic environment for bedrock diagenesis at Meridiani Planum on Mars, *Nature*, *438*, 1129–1131, doi:10.1038/nature04390.

McLennan, S. M., et al. (2005), Provenance and diagenesis of the evaporite-bearing Burns formation, Meridiani Planum, Mars, *Earth Planet. Sci. Lett.*, *240*, doi:10.1016/j.epsl.2005.09.041.

Morris, R. V., et al. (2006), Mossbauer mineralogy of rock, soil, and dust at Meridiani Planum, Mars: Opportunity's journey across sulfate-rich outcrop, basaltic sand and dust, and hematite lag deposits, *J. Geophys. Res.*, *111*, E12S15, doi:10.1029/2006JE002791.

Reid, R. J., et al. (1999), Imager for Mars Pathfinder (IMP) image calibration, *J. Geophys. Res.*, *104*, 8907–8926.

Rieder, R., R. Gellert, J. Brückner, G. Klingelhöfer, G. Dreibus, A. Yen, and S. W. Squyres (2003), The new Athena Alpha Particle X-Ray Spectrometer for the Mars Exploration Rovers, *J. Geophys. Res.*, *108*(E12), 8066, doi:10.1029/2003JE002150.

Rieder, R., et al. (2004), Chemistry of rocks and soils at Meridiani Planum from the Alpha Particle X-ray Spectrometer, *Science*, *306*, 1746–1749, doi:10.1126/science.1104358.

Ruff, S. W., P. R. Christensen, T. D. Glotch, D. L. Blaney, J. E. Moersch, and M. B. Wyatt (2008), The mineralogy of Gusev Crater and Meridiani Planum derived from the Miniature Thermal Emission Spectrometers on the Spirit and Opportunity rovers, in *The Martian Surface: Composition, Mineralogy, and Physical Properties*, edited by J. F. Bell III, pp. 315–338, Cambridge Univ. Press, New York, doi:10.1017/CBO9780511536076.015.

Schröder, C., et al. (2008), Meteorites on Mars observed with the Mars Exploration Rovers, *J. Geophys. Res.*, *113*, E06S22, doi:10.1029/2007JE002990.

Schröder, C., et al. (2010), Properties and distribution of paired stony meteorite candidate rocks at Meridiani Planum, Mars, *J. Geophys. Res.*, doi:10.1029/2010JE003616, in press.

Squyres, S. W., et al. (2004), The Opportunity rover's Athena Science investigation at Meridiani Planum, Mars, *Science*, *306*, 1698–1703, doi:10.1126/science.1106171.

Squyres, S. W., et al. (2006), Overview of the Opportunity Mars Exploration Rover Mission to Meridiani Planum: Eagle Crater to Purgatory Ripple, *J. Geophys. Res.*, *111*, E12S12, doi:10.1029/2006JE002771.

Weitz, C. M., R. C. Anderson, J. F. Bell III, W. H. Farrand, K. E. Herkenhoff, J. R. Johnson, B. L. Jolliff, R. V. Morris, S. W. Squyres, and R. J. Sullivan (2006), Soil grain analyses at Meridiani Planum, Mars, *J. Geophys. Res.*, *111*, E12S04, doi:10.1029/2005JE002541.

Yingst, R. A., L. Crumpler, W. H. Farrand, R. Li, N. A. Cabrol, and L. D. Neakrase (2008), Morphology and texture of particles along the Spirit rover traverse from sol 450 to sol 745, *J. Geophys. Res.*, *113*, E12S41, doi:10.1029/2008JE003179.

Zipfel, J., et al. (2010), Bounce Rock-A Shergottite-like Basalt Encountered at Meridiani Planum, Mars, *Meteorit. Planet. Sci.*, in press.

J. Ashley, Mars Space Flight Facility, Arizona State University, Tempe, AZ 85287, USA.

J. Bell, Department of Astronomy, Cornell University, 428 Space Sciences Bldg., Ithaca, NY 14853, USA.

W. Calvin, Department of Geological Science and Engineering, University of Nevada, Reno, NV 89557, USA.

B. Cohen, NASA Marshall Space Flight Center, VP62, 320 Sparkman Dr., Huntsville, AL 35805, USA.

W. H. Farrand, Space Science Institute, 4750 Walnut St., Ste. 205, Boulder, CO 80301, USA.

I. Fleischer and G. Klingelhöfer, Institut für Anorganische Chemie und Analytische Chemie, Johannes Gutenberg-Universität, Staudinger Weg 9, D-55128 Mainz, Germany.

R. Gellert, Department of Physics, University of Guelph, Guelph, ON N1G 2W1, Canada.

K. E. Herkenhoff and J. R. Johnson, Astrogeology Science Center, U.S. Geological Survey, 2255 N. Gemini Dr., Flagstaff, AZ 86001, USA.

B. Jolliff, Department of Earth and Planetary Sciences, Washington University in St. Louis, One Brookings Drive, St. Louis, MO 63130, USA.

M. Rutherford, Department of Geological Sciences, Brown University, Providence, RI 02912, USA.

C. Schröder, Center for Applied Geoscience, Eberhard Karls University of Tübingen, Sigwartstr. 10, D-72076 Tübingen, Germany.

C. M. Weitz and A. Yingst, Planetary Science Institute, 1700 East Fort Lowell, Ste. 106, Tucson, AZ 85719, USA. (weitz@psi.edu)